

# Ion energy distributions and sheath voltages in a radio-frequency-biased, inductively coupled, high-density plasma reactor

Mark A. Sobolewski,<sup>a)</sup> James K. Olthoff, and Yicheng Wang  
National Institute of Standards and Technology, Gaithersburg, Maryland 20899

(Received 20 November 1998; accepted for publication 14 January 1999)

Ion energy distributions were measured at a grounded surface in an inductively coupled, high-density plasma reactor for pure argon, argon-helium, and argon-xenon discharges at 1.33 Pa (10 mTorr), as a function of radio-frequency (rf) bias amplitude, rf bias frequency, radial position, inductive source power, and ion mass. The ground sheath voltage which accelerates the ions was also determined using capacitive probe measurements and Langmuir probe data. Together, the measurements provide a complete characterization of ion dynamics in the sheath, allowing ion transit time effects to be distinguished from sheath impedance effects. Models are presented which describe both effects and explain why they are observed in the same range of rf bias frequency. [S0021-8979(99)03808-6]

## I. INTRODUCTION

In high-density plasma reactors used for materials processing, plasmas are generated by inductive sources,<sup>1</sup> electron cyclotron resonance (ECR) sources,<sup>2</sup> or helicon sources.<sup>3</sup> In addition, the substrate electrode is also usually powered by a separate, capacitively coupled "radio-frequency (rf) bias" power supply, which controls the kinetic energy of ions bombarding the substrate. When rf bias is applied, rf voltage is dropped across the space-charge sheath adjacent to the substrate electrode, and ions are accelerated to higher energies as they cross the sheath. In addition, part of the applied rf bias voltage is dropped across the opposing sheath, which is adjacent to grounded reactor surfaces (or any other surfaces that act as the rf counterelectrode). This produces an increase in the energy of ions bombarding the grounded surfaces. Crucial process parameters such as oxide etch selectivity depend on ion bombardment energies at the substrate. Ion bombardment of grounded surfaces is also important, because it wastes power and may damage those surfaces. Also, species desorbed or sputtered from reactor surfaces undergoing ion bombardment may be transported to the substrate, and may contaminate it.

Ion kinetic energy distributions have been measured in high-plasma-density discharges generated by planar, inductively coupled sources,<sup>4-9</sup> ECR sources,<sup>10-14</sup> and helicons<sup>14-18</sup> in argon,<sup>4-7,9-13,15-18</sup> chlorine,<sup>8</sup> argon-chlorine mixtures,<sup>9</sup> and HBr.<sup>14</sup> These studies have investigated the dependence of ion energy on pressure,<sup>4-12,14-16</sup> source power,<sup>5-9,11,12,14-16,18</sup> radial position,<sup>6,7</sup> axial position,<sup>15-18</sup> gas mixture,<sup>9</sup> reactor aging,<sup>8</sup> and applied magnetic fields.<sup>10-12,16,17</sup> Nevertheless, the dependence of ion energy on rf bias amplitude and frequency has not been investigated in sufficient detail. Of all of the studies cited above, only three<sup>11,13,14</sup> report ion energy distributions measured with rf bias applied.

The dependence of ion energies on rf bias frequency is particularly important. When the rf bias frequency in an ECR reactor was increased from 0.5 to 20 MHz, the width of the Ar<sup>+</sup> ion energy distribution measured at the rf-biased electrode narrowed from 37 to 5 eV.<sup>11</sup> This narrowing, which has also been observed at a grounded electrode in an ECR reactor<sup>13</sup> and in low-plasma-density, capacitively coupled discharges,<sup>19-21</sup> is explained by ion transit time effects. At low frequencies, the time it takes ions to cross the sheath is short compared to the rf period, so the final energy of an ion varies depending on the time that the ion entered the sheath. Ions entering the sheath when the sheath voltage is high gain more energy than ions entering the sheath when the sheath voltage is low. In contrast, at high rf bias frequencies, ions take many rf periods to cross the sheath, so that the final energy of an ion does not depend strongly on the time at which the ion enters the sheath. Consequently the ion energy distribution narrows as the rf bias frequency increases.

The rf bias frequency also affects the impedance of the sheaths, which in turn determines how symmetrically the rf bias voltage is divided between them. This phenomenon has been extensively studied in capacitively coupled discharges.<sup>22-26</sup> More recently, sheath impedances in a high-density discharge have been measured.<sup>27</sup> In that study, the fraction of the applied rf bias voltage that is dropped across the ground sheath decreased dramatically as the rf bias frequency increased from 0.1 to 10 MHz. Presumably, this phenomenon would have large effects on the energy distribution of ions at grounded surfaces. Like the ion transit time mechanism, it too could produce a narrowing at high frequencies.

In this study, we investigated the role of rf bias frequency on ion energies in the same high-density reactor as Ref. 27. Ion energies at grounded surfaces were measured, and the ground sheath voltage which accelerates these ions was determined using capacitive probe measurements and Langmuir probe data. Taken together, the measurements allow us to distinguish ion transit time effects from sheath impedance effects. Models are presented which describe both

<sup>a)</sup>Electronic mail: sobo@enh.nist.gov

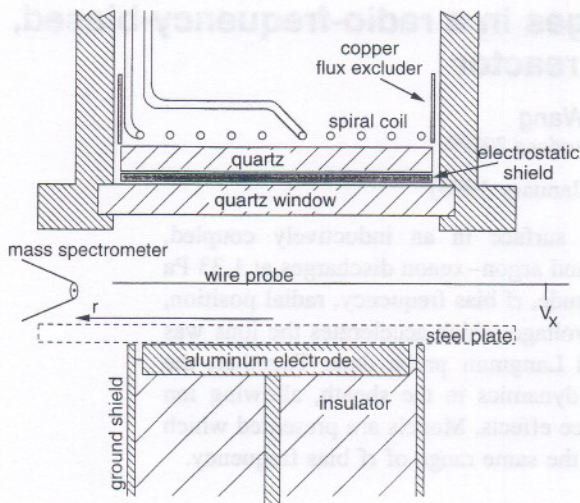


FIG. 1. (a) Diagram of the inductively coupled GEC cell. The orientation of the mass spectrometer sampling cone and the wire probe are also depicted.

types of effects and explain why they are observed in the same frequency range.

## II. EXPERIMENTAL APPARATUS

Experiments were performed in a gaseous electronics conference (GEC) reference cell<sup>28</sup> (Fig. 1), in which the standard upper electrode was replaced by an inductive, high-density plasma source. The source<sup>29</sup> is a five-turn, planar coil, grounded at one end and driven at the other end by a 13.56 MHz rf generator at power levels ranging from 75 to 250 W. (Power values reported here, measured at the generator, include resistive losses in the matching elements and in the planar coil itself.) An electrostatic shield<sup>30</sup> was placed below the coil, insulated from it by a quartz disk. Another quartz disk beneath the shield was sealed to the vacuum chamber. Gas flowed into the cell through a 2.75 in. side port at a total flow rate of 5.0 sccm for argon and argon-helium, 51.0 sccm for argon-xenon. The gas outlet was a 6 in. port on which a turbo pump was mounted. Pressure in the cell was controlled at 1.33 Pa (10 mTorr) by varying the rotation speed of the turbo.

Ion kinetic energy distributions were measured using a Vacuum Generators SXP300H<sup>31</sup> quadrupole mass spectrometer (MS) equipped with a cylindrical mirror analyzer (CMA) ion energy analyzer. This apparatus has been used previously in a capacitively coupled GEC cell<sup>32</sup> and in a direct-current (dc) Townsend discharge.<sup>33</sup> Here, the CMA-MS system was mounted to a 6 in. side port of the inductively coupled GEC cell via a bellows, so that ions could be sampled from the side of the plasma, at variable radial positions. Ions were sampled through a small orifice (0.2 mm diameter) in the grounded, stainless steel sampling cone, then energy analyzed by the CMA, and mass analyzed by the quadrupole mass spectrometer. The ion energy distributions were measured by setting the quadrupole to pass ions of a specific mass and then scanning the energy of the ions allowed through the CMA. The energy resolution of the CMA was held constant at 1 eV for all ions, independent of kinetic energy.

The lower electrode assembly consists of a 10.2-cm-diam. aluminum electrode and a steel ground shield, separated by an alumina insulator. During some of the measurements, as in previous studies,<sup>29,30</sup> a steel plate of diameter 16.5 cm was placed on the lower electrode to increase its effective area. The plate, however, restricted the range of motion of the mass spectrometer. Therefore, we performed additional measurements without the plate.

Radio-frequency bias was applied to the lower electrode of the cell using a signal generator and a power amplifier (Amplifier Research 150A100)<sup>31</sup> as described previously.<sup>27</sup> A Pearson model 2877 current probe<sup>31</sup> and a LeCroy model PP002 voltage probe<sup>31</sup> were mounted on the lead that powered the electrode. Signals acquired by the probes were digitized by an oscilloscope and then transferred to a computer for Fourier analysis. Errors caused by propagation delays and cell parasitics were measured and accounted for, using procedures described previously.<sup>34</sup> These procedures allow us to determine the voltage between the surface of the rf biased electrode and its ground shield,  $V_{pe}(t)$ . In addition, the plasma potential and ground sheath voltage were determined from wire probe measurements, described in the next section.

## III. METHOD: DETERMINING THE PLASMA POTENTIAL AND GROUND SHEATH VOLTAGE

To determine the time-dependent potential in the plasma, a wire probe<sup>35</sup> was inserted into the plasma. A second voltage probe was mounted on the wire, outside vacuum, to measure  $V_x(t)$ , the voltage difference between the wire and the flange on which it was mounted. The potential in the plasma surrounding the wire,  $V_b(t)$ , is given by

$$V_b(t) = V_x(t) + V_{bx}(t), \quad (1)$$

where  $V_{bx}(t)$  is the voltage drop across the sheath that separates the wire from the plasma. Procedures have been developed<sup>36</sup> to determine the rf components of  $V_{bx}(t)$  and  $V_b(t)$  from  $V_x(t)$  measurements. Using these procedures, we verified that, as long as the source was operated in the bright, high-density, inductive mode, rf components of  $V_{bx}(t)$  were  $\leq 0.1$  V, small enough to be neglected.

In contrast, the dc component of  $V_{bx}(t)$  cannot be neglected. This dc component acts to repel plasma electrons from the wire probe, thus maintaining a balance between the flow of electrons and ions from the plasma to the wire. These currents must balance; because the wire probe has a high dc impedance to ground (1 M $\Omega$ ) it draws negligible dc current from the plasma. To repel enough electrons to satisfy the zero net current condition, the dc voltage across the wire probe sheath must be several times the mean kinetic energy of electrons in the vicinity of the wire.

Langmuir probe measurements<sup>29</sup> of the dc plasma potential at zero rf bias, denoted  $V_{bf}$ , and measurements of the dc voltage on the wire probe at zero rf bias,  $V_{xf}$ , determine the dc voltage across the wire probe sheath at zero rf bias,  $V_{bxf}$ .

$$V_{bxf} = V_{bf} - V_{xf}. \quad (2)$$

When rf bias is applied, the dc plasma potential and the dc voltage on the wire probe will change, but the dc voltage

across the wire sheath will not change (unless the rf bias perturbs the local electron energies in the vicinity of the wire probe). Thus, with or without rf bias, the plasma potential  $V_b(t)$  can be determined from

$$V_b(t) = V_x(t) + V_{bxf}. \quad (3)$$

Nearly all of the rf bias voltage is dropped across the sheaths, either the powered sheath or the ground sheath, and not across the much more conductive plasma. Therefore, we expect spatial variations in the plasma potential to be small, at least for the components at the rf bias frequency and its harmonics. (The harmonics are generated by the nonlinear properties of the sheath, not the plasma). Because the intertwined loops and support wire that constitute the wire probe span a wide range of radial and azimuthal positions, it is not able to resolve radial and azimuthal variations. Nevertheless, axial variations in the rf components of the plasma potential were measured, and were found to be small, typically 0.1 V, at most 2 V, even at hundreds of volts of rf bias. Spatial variations in the dc component of the plasma potential are larger, on the order of 10 V, according to Langmuir probe studies,<sup>29,30</sup> but these variations are accounted for using Eqs. (2) and (3). To determine the plasma potential at a particular position from Eq. (3), one need only insert the value of  $V_{bf}$  measured at that position into Eq. (2). In particular, we may use Eq. (3) to determine the plasma potential in the vicinity of the mass spectrometer sampling cone. Since the cone is grounded, we can also obtain the voltage drop across the sampling cone sheath,  $V_{gs}(t)$ , from

$$V_{gs}(t) = V_b(t). \quad (4)$$

This equation neglects any electromotive force (emf) in the circuit consisting of the wire probe, the mass spectrometer, and the vacuum chamber wall. This circuit lies in the horizontal plane, so it should not enclose any appreciable magnetic flux generated by the rf bias current, which flows through the plasma in a generally vertical direction.

## IV. RESULTS

### A. No rf bias

Figure 2(a) shows a kinetic energy distribution for  $\text{Ar}^+$  ions, measured when no rf bias was applied, for a discharge in 1.33 Pa (10 mTorr) of argon at an inductive source power of 100 W. The distribution consists of a single narrow peak.  $\text{Ar}^+$  energy distributions measured at higher pressures in capacitively coupled discharges<sup>32,37-46</sup> display multiple peaks and contributions near zero ion energy, which are attributed to ions that have lost energy due to collisions in the sheath. No such features are seen in Fig. 2(a), indicating that ions cross the sheath in front of the sampling cone without undergoing collisions. Collisions in the sheath are negligible because the sheath width is much thinner than the ion mean free path. In high-density discharges, sheath widths are on the order of 100  $\mu\text{m}$ , while the mean free path of  $\text{Ar}^+$  due to the dominant collision process,  $\text{Ar}-\text{Ar}^+$  charge exchange, is 5–7 mm at 1.33 Pa, according to measured cross sections<sup>47</sup> of 1–10 eV ions. In fact, the mean free path is so long that ions may also cross the presheath region without colliding.

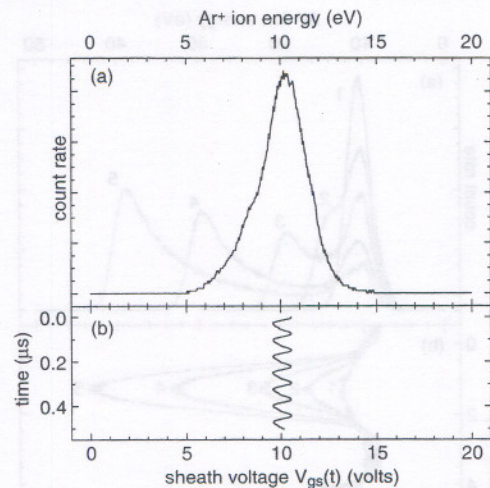


FIG. 2. (a)  $\text{Ar}^+$  kinetic energy distribution for a pure argon discharge at 1.33 Pa (10 mTorr), an inductive source power of 100 W, and a radial position  $r=9$  cm, without rf bias. (b) Wave form of the voltage across the ground sheath,  $V_{gs}(t)$ , obtained at the same conditions.

For this reason, and for the sake of simplicity, the presheath will be considered part of the sheath in the remainder of this article.

Although ion collisions in the sheath can be neglected, ion collisions in the plasma cannot. In Fig. 2, the sampling cone is located at a radial position  $r=9$  cm. Ions created near  $r=0$ , the radial center of the discharge, undergo many collisions before reaching the sample cone sheath. Although Langmuir probe measurements<sup>29,30</sup> indicate that the plasma supports a radial electric field which accelerates  $\text{Ar}^+$  ions away from the center of the discharge, much of the momentum that ions gain from the field is redirected in random directions by  $\text{Ar}-\text{Ar}^+$  collisions. By assuming that the ions are in equilibrium with the local electric field, obtained from Miller's Langmuir probe data,<sup>29</sup> Hebner<sup>48</sup> calculated that  $\text{Ar}^+$  ions at radial positions of 4–8 cm have a radial drift velocity of about  $1 \times 10^5$  cm/s, which corresponds to an energy of only 0.2 eV. Laser-induced fluorescence measurements<sup>48</sup> of the drift velocity of argon metastable ions in the plasma were higher, ranging up to  $2.5 \times 10^5$  cm/s. This corresponds to an energy of 1.3 eV, which is still low compared to the energies in Fig. 2. Thus the ions gain nearly all of their energy in the sheath rather than the plasma.

Figure 2(b) shows the wave form of the voltage across the ground sheath,  $V_{gs}(t)$ , obtained at the same conditions as Fig. 2(a), using wire probe measurements and Eqs. (2)–(4). The voltage scale in Fig. 2(b) coincides with the energy scale of Fig. 2(a). The energy,  $E_0$ , of the peak in the energy distribution function closely corresponds to  $V_{dc}$ , the dc component of  $V_{gs}(t)$ . This observation confirms that the ions gain nearly all of their energy in the sheath rather than the plasma. Since no rf bias is applied, the only rf components observed in Fig. 2(b) are at the inductive source frequency and its harmonics. These components, which arise from a capacitive coupling between the inductive source and the plasma, are small, about 1 V, as noted in previous studies.<sup>27,29</sup> This 1 V modulation in  $V_{gs}(t)$  contributes to the width of the ion energy distribution. The distribution has a full-width at half-

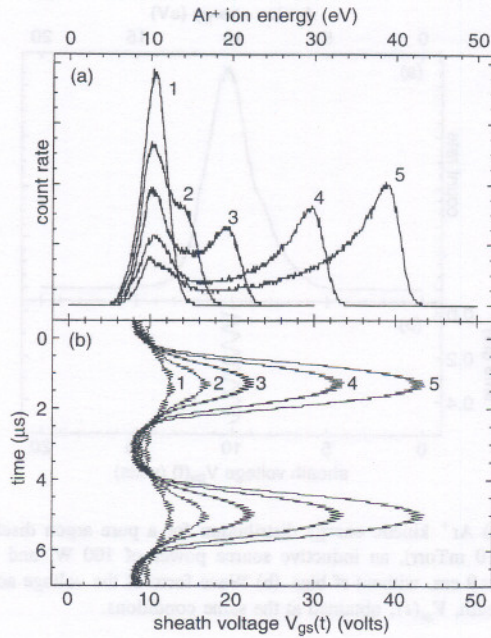


FIG. 3. (a) Ar<sup>+</sup> kinetic energy distribution for a pure argon discharge at 1.33 Pa (10 mTorr), an inductive source power of 100 W, a radial position  $r=9$  cm, and a bias frequency of 0.27 MHz, for varying rf bias amplitudes. (b) Wave forms of the voltage across the ground sheath,  $V_{gs}(t)$ , obtained under the same conditions.

maximum of 2.5 eV. About 1 eV of this width is contributed by the energy resolution of the energy analyzer. The remainder is contributed by the modulation in  $V_{gs}(t)$  and by the angular distribution of ion velocities within the plasma.

**B. Low frequency rf bias**

Figure 3(a) shows ion energy distributions measured with rf bias applied at 0.27 MHz, at varying rf bias amplitudes. The distributions in Fig. 3(a) are broader than the distribution observed at zero rf bias [see Fig. 2(a)]. At the lowest rf bias amplitude, the distribution has a full-width at half-maximum of 3.3 eV, 0.8 eV broader than in Fig. 2(a). As the rf bias amplitude increases, the distribution continues to broaden and a double-peaked structure appears. The energy of the higher-energy peak increases with rf bias amplitude, but the position of the lower-energy peak remains constant. The lower-energy peak always lies close to  $E_0$ , the energy of the single peak in the distribution observed at zero rf bias [see Fig. 2(a)]. The double-peaked distributions are similar to previous measurements performed at low pressures and low frequencies.<sup>11,13,21,49</sup>

Figure 3(b) shows corresponding wave forms for the ground sheath voltage,  $V_{gs}(t)$ . The high frequency “ripple” visible in each wave form, independent of rf bias, is contributed by Fourier components at the inductive source frequency (13.56 MHz) and its harmonics, which are produced by capacitive coupling from the coil. The lower frequency features are contributed by Fourier components at the rf bias frequency and its harmonics. As the rf bias amplitude increases, the maximum wire probe voltage,  $V_{max}$ , becomes larger, reaching more than 40 V in Fig. 4(b), but the minimum wire probe voltage,  $V_{min}$ , decreases only slightly. This

behavior parallels that observed in Fig. 3(a). The energy of the higher-energy peak in the distributions,  $E_{high}$ , varies in the same manner as  $V_{max}$ ;  $E_{high}$  always lies a few electron volts below  $eV_{max}$  (where  $e$  is the charge of an electron). Similarly, the energy of the lower-energy peak in the distributions,  $E_{low}$ , lies a few electron volts above  $eV_{min}$ . The separation between the peaks,  $\Delta E_k$ , closely tracks the peak-to-peak amplitude of the ground sheath voltage,  $V_{pp}$ .

The correlations between Figs. 3(a) and 3(b) suggest that ions cross the sheath in front of the sampling cone rapidly compared to the time scale of Fig. 3(b). If so, ions entering the sheath at time  $t_0$ , when the instantaneous voltage across the sheath is  $V_{gs}(t_0)$ , will gain an energy  $eV_{gs}(t_0)$  in crossing the sheath. If they enter the sheath with low kinetic energies  $\ll eV_{gs}(t_0)$ , as argued in Sec. IV A above, they will exit the sheath and enter the mass spectrometer with a kinetic energy equal to  $eV_{gs}(t_0)$ . If ions enter the sheath at all times, then ions will be observed at all energies between  $eV_{max}$  and  $eV_{min}$ . The peaks at  $E_{max} \approx eV_{max}$  and  $E_{min} \approx eV_{min}$  are observed because  $V_{gs}(t)$  varies rather slowly near its maximum and minimum. Because  $V_{gs}(t)$  sweeps more rapidly through intermediate voltages, fewer ions are collected at intermediate energies.

The time it takes the ions to cross the sheath can be estimated using dc sheath models. The voltage drop across a dc sheath,  $V_0$ , is independent of time. At any position,  $x$ , in the sheath the potential,  $V(x)$ , is also independent of time. If the boundary between the plasma and the sheath is at  $x=0$  and if the electrode or other grounded surface is at  $x=W$ , then  $V(0)=V_0$ , and  $V(W)=0$ . If the ions have negligible initial velocity, then  $u(x)$ , the velocity of ions at position  $x$ , will be given by

$$\frac{1}{2} m_i u^2(x) = -eV(x) + eV_0, \tag{5}$$

where  $m_i$  is the ion mass. Using this equation, Poisson’s equation, and the ion continuity equation (with the electric field at  $x=0$ , the electron density in the sheath, and the density of other ionic species all set to zero) one can solve for  $V(x)$ . The solution is the Child–Langmuir law,<sup>50</sup>

$$x = \frac{2}{3} (2e/m_i)^{1/4} (\epsilon_0/J_0)^{1/2} [V_0 - V(x)]^{3/4}, \tag{6}$$

where  $\epsilon_0$  is the permittivity of vacuum and  $J_0$  is the ion current density. Evaluating Eq. (6) at  $x=W$ , one obtains

$$W = \frac{2}{3} (2e/m_i)^{1/4} (\epsilon_0/J_0)^{1/2} V_0^{3/4}. \tag{7}$$

Sometimes the ion transit time,  $\tau$ , is estimated by assuming ions cross the entire sheath at their maximum velocity,  $u_{max} = (2eV_0/m_i)^{1/2}$ . One obtains

$$\tau = W/u_{max} = \frac{2}{3} (m_i V_0/2e)^{1/4} (\epsilon_0/J_0)^{1/2}. \tag{8}$$

A more accurate estimate is obtained by integration. If  $y(t)$  is the position of an ion as a function of time, then the ion velocity as a function of time is  $dy/dt = u(y)$ , and the transit time is

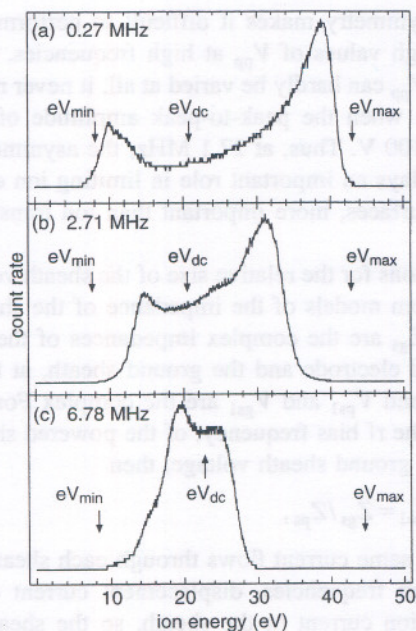


FIG. 4. (a)  $\text{Ar}^+$  kinetic energy distribution for a pure argon discharge at 1.33 Pa (10 mTorr), an inductive source power of 100 W, a radial position  $r=9$  cm, and rf bias frequencies of (a) 0.27, (b) 2.71 and (c) 6.78 MHz. Arrows indicate energies that correspond to  $V_{\min}$ ,  $V_{\max}$ , and  $V_{\text{dc}}$ , the minimum, maximum and dc values of the ground sheath voltage,  $V_{\text{gs}}(t)$ .

$$\tau = \int_0^W u^{-1}(y) dy = \int_0^W (2eV(y)/m_i)^{-1/2} dy. \quad (9)$$

Substituting Eqs. (5)–(7) into Eq. (9),

$$\tau = 2(m_i V_0 / 2e)^{1/4} (\epsilon_0 / J_0)^{1/2}. \quad (10)$$

Transit times for rf sheaths can be estimated with this equation by replacing  $V_0$ , the dc sheath voltage, with  $V_{\text{gs}}(t_0)$ , the value of the sheath voltage at a given time. An average transit time can be obtained by replacing  $V_0$  with  $V_{\text{dc}}$ , the dc voltage across the rf sheath. In either case, a value for the ion current density,  $J_0$ , is required. Fortunately, the ion current density has been measured in an inductive GEC cell, for 1.33 Pa argon discharges at an inductive source power of 100 W, using a miniaturized, gridded ion detector.<sup>7</sup> Using the value  $0.5 \text{ mA/cm}^2$  measured at a radial position,  $r=8$  cm, close to the position of the sampling cone, and the 10–40 V range of sheath voltages shown in Fig. 3(b), transit times from 100 to 200 ns are obtained. These calculated transit times are indeed small compared to the time scale of Fig. 3. The 0.27 MHz rf bias frequency used in Fig. 3 corresponds to an rf period,  $T$ , of  $3.7 \mu\text{s}$ , thus  $\tau$  is only 2.7%–5.5% of  $T$ .

### C. High frequency rf bias

Figure 4 shows  $\text{Ar}^+$  ion energy distributions measured at varying rf bias frequencies. At each frequency, the rf bias amplitude was adjusted so that  $V_{\text{pp}}$ , the peak-to-peak amplitude of the ground sheath voltage, was nearly constant, within one volt of 35.5 V. As the frequency increases from Fig. 4(a) to 4(c), the distribution becomes narrower, the lower energy peak shifts to higher energy, and the higher

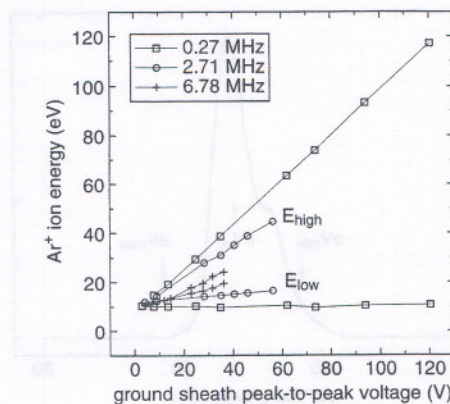


FIG. 5. Energy of the higher energy peak in the  $\text{Ar}^+$  distribution,  $E_{\text{high}}$ , and the lower energy peak,  $E_{\text{low}}$ , as a function of  $V_{\text{pp}}$ , the peak-to-peak amplitude of the ground sheath voltage, and the rf bias frequency. In some cases at 6.78 MHz a single energy is plotted because only a single peak was observed. Data were obtained for a pure argon discharge at 1.33 Pa (10 mTorr), an inductive source power of 100 W, and a radial position  $r=9$  cm.

energy peak shifts to lower energy. In Fig. 4(c), at 6.78 MHz, the peaks are so close that it is difficult to resolve them. For each distribution, arrows mark the energies  $eV_{\min}$ ,  $eV_{\max}$ , and  $eV_{\text{dc}}$ , which correspond to the minimum, maximum, and dc component of the ground sheath voltage. As the frequency increases,  $E_{\text{high}}$  shifts from the vicinity of  $eV_{\max}$  towards  $eV_{\text{dc}}$ , and  $E_{\text{low}}$  shifts from the vicinity of  $eV_{\min}$  towards  $eV_{\text{dc}}$ .

Data from varying rf bias frequencies and amplitudes are shown in Fig. 5. There, the peak energies,  $E_{\text{high}}$  and  $E_{\text{low}}$ , are plotted versus  $V_{\text{pp}}$ , the peak-to-peak amplitude of the ground sheath voltage. At 0.27 MHz,  $E_{\text{high}}$  varies linearly with  $V_{\text{pp}}$  and  $E_{\text{low}}$  is relatively insensitive to  $V_{\text{pp}}$ , as noted in Sec. IV B and Fig. 3, above. As the frequency is increased, however, the slope of the  $E_{\text{high}}$  plots become less steep and the slope of  $E_{\text{low}}$  becomes more steep. Thus, at constant  $V_{\text{pp}}$ , the separation between  $E_{\text{high}}$  and  $E_{\text{low}}$  becomes smaller as the frequency increases, as in Fig. 4.

The narrowing of the ion energy distribution at high frequencies seen in Figs. 4 and 5 is similar to measurements made in ECR reactors,<sup>11,13</sup> measurements made in capacitively coupled cells,<sup>20,21</sup> and predictions obtained from computer simulations.<sup>13,51,52</sup> The narrowing is expected whenever the ion transit time becomes comparable to the rf period. Here, the ratio of the ion transit time,  $\tau$ , obtained from Eq. (10), to the rf period,  $T$ , is about 0.3 at 2.71 MHz, and 0.8 at 6.78 MHz. Thus, at these frequencies, the time that an ion spends in the sheath is a large fraction of the rf period. Consequently, the energy that ions gain in the sheath is no longer given by the instantaneous sheath voltage; rather, it is given by an average value of the sheath voltage, averaged over the time that the ion spends in the sheath. This averaging reduces the maximum ion energy and raises the minimum ion energy. Hence the distribution becomes narrower. If the frequency is high enough that the ion transit time is much greater than the rf period, the ions will experience nearly the same total acceleration no matter when they enter the sheath, and only a single peak will be observed in

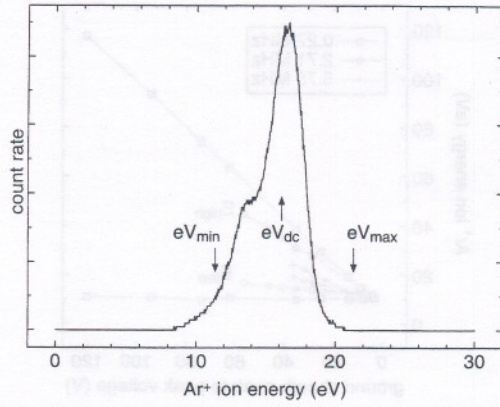


FIG. 6. Ar<sup>+</sup> kinetic energy distribution for a pure argon discharge at 1.33 Pa (10 mTorr), an inductive source power of 100 W, a radial position  $r = 9$  cm, and an rf bias frequency of 27.12 MHz. Arrows indicate energies that correspond to  $V_{\min}$ ,  $V_{\max}$ , and  $V_{dc}$ , the minimum, maximum, and dc values of the ground sheath voltage,  $V_{gs}(t)$ .

the ion energy distribution, at an energy equal to  $eV_{dc}$ . Indeed, Ar<sup>+</sup> energy distributions measured at 27.1 MHz, where  $\tau/T \approx 3$ , do not show two clearly defined peaks; they only show a single peak with a shoulder at lower energies (Fig. 6). It should be noted, however, that the amplitude of the ground sheath voltage in Fig. 6, indicated by the arrows, is rather small. Large amplitudes for the ground sheath voltage could not be obtained by rf biasing at 27.1 MHz, for reasons that are explained in the next section.

**D. Discharge symmetry**

In Fig. 7,  $V_{pp}$ , the peak-to-peak amplitude of the ground sheath voltage, is plotted as a function of the peak-to-peak amplitude of  $V_{pe}(t)$ , the voltage applied to the rf biased electrode. At low rf bias frequencies the discharge is relatively symmetric, that is,  $V_{pp}$  is a large fraction of the peak-to-peak applied voltage, comparable to the peak-to-peak voltage across the sheath at the rf biased electrode (not shown). As the rf bias frequency increases,  $V_{pp}$  becomes a smaller and smaller fraction of the peak-to-peak applied voltage, making the discharge less symmetric. Similar behavior is observed in plots<sup>27</sup> of the fundamental amplitudes of  $V_{gs}(t)$  and  $V_{pe}(t)$  (i.e., the magnitude of their Fourier components at the rf bias frequency) and in plots of their peak amplitudes. The in-

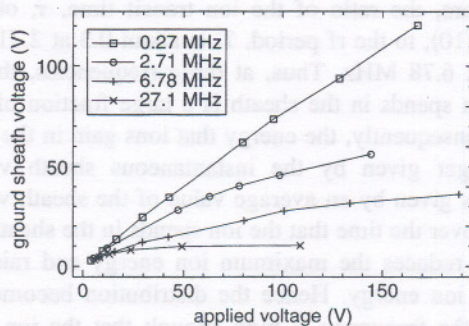


FIG. 7. Peak-to-peak amplitude of the ground sheath voltage,  $V_{pp}$ , plotted on the y axis, as a function of the peak-to-peak amplitude of the voltage on the rf biased electrode,  $V_{pe}(t)$ , for varying rf bias frequencies.

creasing asymmetry makes it difficult to perform measurements at high values of  $V_{pp}$  at high frequencies. Indeed, at 27.1 MHz  $V_{pp}$  can hardly be varied at all: it never rises above 11 V, even when the peak-to-peak amplitude of  $V_{pe}(t)$  is more than 100 V. Thus, at 27.1 MHz, the asymmetry of the discharge plays an important role in limiting ion energies at grounded surfaces, more important than ion transit time effects.

Predictions for the relative size of the sheath voltages are obtained from models of the impedance of the sheaths.<sup>22-26</sup> If  $Z_{ps}$  and  $Z_{gs}$  are the complex impedances of the sheath at the powered electrode and the ground sheath, at the rf bias frequency, and  $V_{ps1}$  and  $V_{gs1}$  are the complex Fourier coefficients, at the rf bias frequency, of the powered sheath voltage and the ground sheath voltage, then

$$V_{gs1}/V_{ps1} = Z_{gs}/Z_{ps}, \tag{11}$$

because the same current flows through each sheath. At sufficiently high frequencies, displacement current dominates the conduction current in the sheath, so the sheath impedances are largely capacitive. The capacitive sheath impedance,  $Z$ , can be estimated as

$$Z = W/(i\epsilon_0\omega A) = \frac{2}{3} (2e/m_i)^{1/4} (J_0\epsilon_0)^{-1/2} V_0^{3/4} / (i\omega A), \tag{12}$$

where  $\omega$  is the rf bias frequency in radians per second and  $A$  is the area of the sheath. This result is derived from the Child-Langmuir law, Eq. (7), which is strictly valid only for a dc sheath, but a nearly identical result, differing only by a multiplicative factor, is obtained from a high-frequency sheath model.<sup>53</sup> From Eqs. (11) and (12), one obtains

$$V_{gs1}/V_{ps1} = (J_{ps}/J_{gs})^2 (A_{ps}/A_{gs})^4. \tag{13}$$

where  $A_{gs}$ ,  $A_{ps}$ ,  $J_{gs}$ , and  $J_{ps}$  denote the area and the ion current density of the ground sheath and the powered electrode sheath. If one assumes that  $J_{ps} = J_{gs}$ , one obtains the scaling law derived by Koenig and Maisel<sup>22</sup> and by Lieberman,<sup>26</sup> in which the ratio of the sheath voltages varies as the fourth power of the area ratio. This strong dependence on the area ratio, and the large grounded area in the inductive GEC cell, explain why  $V_{gs1}/V_{ps1}$  is small at high rf bias frequencies.

At low rf bias frequencies, conduction current dominates the displacement current in the sheath. Because the conductance of the sheaths is nonlinear, the sheaths act like diodes rather than linear resistors. The discharge can be modeled<sup>21</sup> as two diodes, placed back-to-back, with reverse saturation currents  $J_{ps}A_{ps}$  and  $J_{gs}A_{gs}$ . The total current will equal  $J_{gs}A_{gs}$  for a time period  $t_{gs}$ , during which the diode representing the ground sheath is reverse biased, and the total current will equal  $J_{ps}A_{ps}$  for a time period  $t_{ps} = T - t_{gs}$ , during which the powered electrode sheath is reverse biased. Over one rf period,  $T$ , the current must average to zero. Therefore,

$$t_{gs}/t_{ps} = J_{ps}A_{ps}/J_{gs}A_{gs}. \tag{14}$$

If the applied voltage is sinusoidal, then the voltage across each diode is a clipped sinusoid, and the ratio of the peak-to-peak voltage drops across the diodes is

# Ion energy distributions and sheath voltages in a radio-frequency-biased, inductively coupled, high-density plasma reactor

Mark A. Sobolewski,<sup>a)</sup> James K. Olthoff, and Yicheng Wang  
*National Institute of Standards and Technology, Gaithersburg, Maryland 20899*

(Received 20 November 1998; accepted for publication 14 January 1999)

Ion energy distributions were measured at a grounded surface in an inductively coupled, high-density plasma reactor for pure argon, argon-helium, and argon-xenon discharges at 1.33 Pa (10 mTorr), as a function of radio-frequency (rf) bias amplitude, rf bias frequency, radial position, inductive source power, and ion mass. The ground sheath voltage which accelerates the ions was also determined using capacitive probe measurements and Langmuir probe data. Together, the measurements provide a complete characterization of ion dynamics in the sheath, allowing ion transit time effects to be distinguished from sheath impedance effects. Models are presented which describe both effects and explain why they are observed in the same range of rf bias frequency. [S0021-8979(99)03808-6]

## I. INTRODUCTION

In high-density plasma reactors used for materials processing, plasmas are generated by inductive sources,<sup>1</sup> electron cyclotron resonance (ECR) sources,<sup>2</sup> or helicon sources.<sup>3</sup> In addition, the substrate electrode is also usually powered by a separate, capacitively coupled "radio-frequency (rf) bias" power supply, which controls the kinetic energy of ions bombarding the substrate. When rf bias is applied, rf voltage is dropped across the space-charge sheath adjacent to the substrate electrode, and ions are accelerated to higher energies as they cross the sheath. In addition, part of the applied rf bias voltage is dropped across the opposing sheath, which is adjacent to grounded reactor surfaces (or any other surfaces that act as the rf counterelectrode). This produces an increase in the energy of ions bombarding the grounded surfaces. Crucial process parameters such as oxide etch selectivity depend on ion bombardment energies at the substrate. Ion bombardment of grounded surfaces is also important, because it wastes power and may damage those surfaces. Also, species desorbed or sputtered from reactor surfaces undergoing ion bombardment may be transported to the substrate, and may contaminate it.

Ion kinetic energy distributions have been measured in high-plasma-density discharges generated by planar, inductively coupled sources,<sup>4-9</sup> ECR sources,<sup>10-14</sup> and helicons<sup>14-18</sup> in argon,<sup>4-7,9-13,15-18</sup> chlorine,<sup>8</sup> argon-chlorine mixtures,<sup>9</sup> and HBr.<sup>14</sup> These studies have investigated the dependence of ion energy on pressure,<sup>4-12,14-16</sup> source power,<sup>5-9,11,12,14-16,18</sup> radial position,<sup>6,7</sup> axial position,<sup>15-18</sup> gas mixture,<sup>9</sup> reactor aging,<sup>8</sup> and applied magnetic fields.<sup>10-12,16,17</sup> Nevertheless, the dependence of ion energy on rf bias amplitude and frequency has not been investigated in sufficient detail. Of all of the studies cited above, only three<sup>11,13,14</sup> report ion energy distributions measured with rf bias applied.

The dependence of ion energies on rf bias frequency is particularly important. When the rf bias frequency in an ECR reactor was increased from 0.5 to 20 MHz, the width of the Ar<sup>+</sup> ion energy distribution measured at the rf-biased electrode narrowed from 37 to 5 eV.<sup>11</sup> This narrowing, which has also been observed at a grounded electrode in an ECR reactor<sup>13</sup> and in low-plasma-density, capacitively coupled discharges,<sup>19-21</sup> is explained by ion transit time effects. At low frequencies, the time it takes ions to cross the sheath is short compared to the rf period, so the final energy of an ion varies depending on the time that the ion entered the sheath. Ions entering the sheath when the sheath voltage is high gain more energy than ions entering the sheath when the sheath voltage is low. In contrast, at high rf bias frequencies, ions take many rf periods to cross the sheath, so that the final energy of an ion does not depend strongly on the time at which the ion enters the sheath. Consequently the ion energy distribution narrows as the rf bias frequency increases.

The rf bias frequency also affects the impedance of the sheaths, which in turn determines how symmetrically the rf bias voltage is divided between them. This phenomenon has been extensively studied in capacitively coupled discharges.<sup>22-26</sup> More recently, sheath impedances in a high-density discharge have been measured.<sup>27</sup> In that study, the fraction of the applied rf bias voltage that is dropped across the ground sheath decreased dramatically as the rf bias frequency increased from 0.1 to 10 MHz. Presumably, this phenomenon would have large effects on the energy distribution of ions at grounded surfaces. Like the ion transit time mechanism, it too could produce a narrowing at high frequencies.

In this study, we investigated the role of rf bias frequency on ion energies in the same high-density reactor as Ref. 27. Ion energies at grounded surfaces were measured, and the ground sheath voltage which accelerates these ions was determined using capacitive probe measurements and Langmuir probe data. Taken together, the measurements allow us to distinguish ion transit time effects from sheath impedance effects. Models are presented which describe both

<sup>a)</sup>Electronic mail: sobo@enh.nist.gov

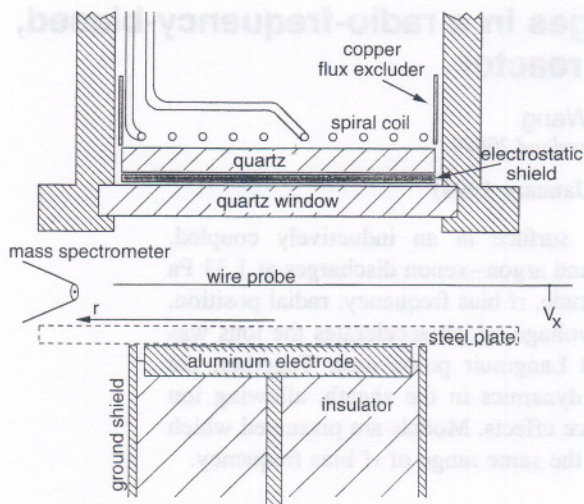


FIG. 1. (a) Diagram of the inductively coupled GEC cell. The orientation of the mass spectrometer sampling cone and the wire probe are also depicted.

types of effects and explain why they are observed in the same frequency range.

## II. EXPERIMENTAL APPARATUS

Experiments were performed in a gaseous electronics conference (GEC) reference cell<sup>28</sup> (Fig. 1), in which the standard upper electrode was replaced by an inductive, high-density plasma source. The source<sup>29</sup> is a five-turn, planar coil, grounded at one end and driven at the other end by a 13.56 MHz rf generator at power levels ranging from 75 to 250 W. (Power values reported here, measured at the generator, include resistive losses in the matching elements and in the planar coil itself.) An electrostatic shield<sup>30</sup> was placed below the coil, insulated from it by a quartz disk. Another quartz disk beneath the shield was sealed to the vacuum chamber. Gas flowed into the cell through a 2.75 in. side port at a total flow rate of 5.0 sccm for argon and argon-helium, 51.0 sccm for argon-xenon. The gas outlet was a 6 in. port on which a turbo pump was mounted. Pressure in the cell was controlled at 1.33 Pa (10 mTorr) by varying the rotation speed of the turbo.

Ion kinetic energy distributions were measured using a Vacuum Generators SXP300H<sup>31</sup> quadrupole mass spectrometer (MS) equipped with a cylindrical mirror analyzer (CMA) ion energy analyzer. This apparatus has been used previously in a capacitively coupled GEC cell<sup>32</sup> and in a direct-current (dc) Townsend discharge.<sup>33</sup> Here, the CMA-MS system was mounted to a 6 in. side port of the inductively coupled GEC cell via a bellows, so that ions could be sampled from the side of the plasma, at variable radial positions. Ions were sampled through a small orifice (0.2 mm diameter) in the grounded, stainless steel sampling cone, then energy analyzed by the CMA, and mass analyzed by the quadrupole mass spectrometer. The ion energy distributions were measured by setting the quadrupole to pass ions of a specific mass and then scanning the energy of the ions allowed through the CMA. The energy resolution of the CMA was held constant at 1 eV for all ions, independent of kinetic energy.

The lower electrode assembly consists of a 10.2-cm-diam. aluminum electrode and a steel ground shield, separated by an alumina insulator. During some of the measurements, as in previous studies,<sup>29,30</sup> a steel plate of diameter 16.5 cm was placed on the lower electrode to increase its effective area. The plate, however, restricted the range of motion of the mass spectrometer. Therefore, we performed additional measurements without the plate.

Radio-frequency bias was applied to the lower electrode of the cell using a signal generator and a power amplifier (Amplifier Research 150A100)<sup>31</sup> as described previously.<sup>27</sup> A Pearson model 2877 current probe<sup>31</sup> and a LeCroy model PP002 voltage probe<sup>31</sup> were mounted on the lead that powered the electrode. Signals acquired by the probes were digitized by an oscilloscope and then transferred to a computer for Fourier analysis. Errors caused by propagation delays and cell parasitics were measured and accounted for, using procedures described previously.<sup>34</sup> These procedures allow us to determine the voltage between the surface of the rf biased electrode and its ground shield,  $V_{pe}(t)$ . In addition, the plasma potential and ground sheath voltage were determined from wire probe measurements, described in the next section.

## III. METHOD: DETERMINING THE PLASMA POTENTIAL AND GROUND SHEATH VOLTAGE

To determine the time-dependent potential in the plasma, a wire probe<sup>35</sup> was inserted into the plasma. A second voltage probe was mounted on the wire, outside vacuum, to measure  $V_x(t)$ , the voltage difference between the wire and the flange on which it was mounted. The potential in the plasma surrounding the wire,  $V_b(t)$ , is given by

$$V_b(t) = V_x(t) + V_{bx}(t), \quad (1)$$

where  $V_{bx}(t)$  is the voltage drop across the sheath that separates the wire from the plasma. Procedures have been developed<sup>36</sup> to determine the rf components of  $V_{bx}(t)$  and  $V_b(t)$  from  $V_x(t)$  measurements. Using these procedures, we verified that, as long as the source was operated in the bright, high-density, inductive mode, rf components of  $V_{bx}(t)$  were  $\leq 0.1$  V, small enough to be neglected.

In contrast, the dc component of  $V_{bx}(t)$  cannot be neglected. This dc component acts to repel plasma electrons from the wire probe, thus maintaining a balance between the flow of electrons and ions from the plasma to the wire. These currents must balance; because the wire probe has a high dc impedance to ground (1 M $\Omega$ ) it draws negligible dc current from the plasma. To repel enough electrons to satisfy the zero net current condition, the dc voltage across the wire probe sheath must be several times the mean kinetic energy of electrons in the vicinity of the wire.

Langmuir probe measurements<sup>29</sup> of the dc plasma potential at zero rf bias, denoted  $V_{bf}$ , and measurements of the dc voltage on the wire probe at zero rf bias,  $V_{xf}$ , determine the dc voltage across the wire probe sheath at zero rf bias,  $V_{bxf}$ .

$$V_{bxf} = V_{bf} - V_{xf}. \quad (2)$$

When rf bias is applied, the dc plasma potential and the dc voltage on the wire probe will change, but the dc voltage

across the wire sheath will not change (unless the rf bias perturbs the local electron energies in the vicinity of the wire probe). Thus, with or without rf bias, the plasma potential  $V_b(t)$  can be determined from

$$V_b(t) = V_x(t) + V_{bxf}. \quad (3)$$

Nearly all of the rf bias voltage is dropped across the sheaths, either the powered sheath or the ground sheath, and not across the much more conductive plasma. Therefore, we expect spatial variations in the plasma potential to be small, at least for the components at the rf bias frequency and its harmonics. (The harmonics are generated by the nonlinear properties of the sheath, not the plasma). Because the intertwined loops and support wire that constitute the wire probe span a wide range of radial and azimuthal positions, it is not able to resolve radial and azimuthal variations. Nevertheless, axial variations in the rf components of the plasma potential were measured, and were found to be small, typically 0.1 V, at most 2 V, even at hundreds of volts of rf bias. Spatial variations in the dc component of the plasma potential are larger, on the order of 10 V, according to Langmuir probe studies,<sup>29,30</sup> but these variations are accounted for using Eqs. (2) and (3). To determine the plasma potential at a particular position from Eq. (3), one need only insert the value of  $V_{bf}$  measured at that position into Eq. (2). In particular, we may use Eq. (3) to determine the plasma potential in the vicinity of the mass spectrometer sampling cone. Since the cone is grounded, we can also obtain the voltage drop across the sampling cone sheath,  $V_{gs}(t)$ , from

$$V_{gs}(t) = V_b(t). \quad (4)$$

This equation neglects any electromotive force (emf) in the circuit consisting of the wire probe, the mass spectrometer, and the vacuum chamber wall. This circuit lies in the horizontal plane, so it should not enclose any appreciable magnetic flux generated by the rf bias current, which flows through the plasma in a generally vertical direction.

## IV. RESULTS

### A. No rf bias

Figure 2(a) shows a kinetic energy distribution for  $\text{Ar}^+$  ions, measured when no rf bias was applied, for a discharge in 1.33 Pa (10 mTorr) of argon at an inductive source power of 100 W. The distribution consists of a single narrow peak.  $\text{Ar}^+$  energy distributions measured at higher pressures in capacitively coupled discharges<sup>32,37-46</sup> display multiple peaks and contributions near zero ion energy, which are attributed to ions that have lost energy due to collisions in the sheath. No such features are seen in Fig. 2(a), indicating that ions cross the sheath in front of the sampling cone without undergoing collisions. Collisions in the sheath are negligible because the sheath width is much thinner than the ion mean free path. In high-density discharges, sheath widths are on the order of 100  $\mu\text{m}$ , while the mean free path of  $\text{Ar}^+$  due to the dominant collision process,  $\text{Ar}-\text{Ar}^+$  charge exchange, is 5-7 mm at 1.33 Pa, according to measured cross sections<sup>47</sup> of 1-10 eV ions. In fact, the mean free path is so long that ions may also cross the presheath region without colliding.

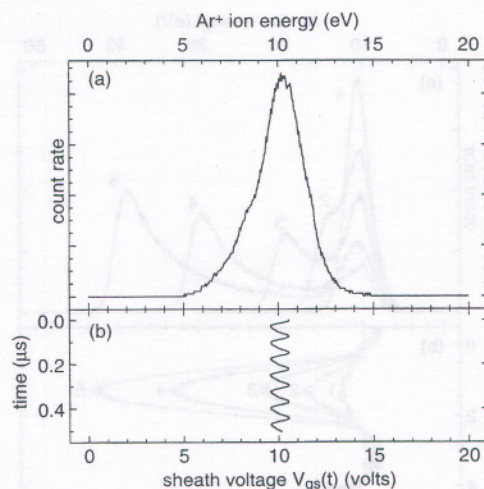


FIG. 2. (a)  $\text{Ar}^+$  kinetic energy distribution for a pure argon discharge at 1.33 Pa (10 mTorr), an inductive source power of 100 W, and a radial position  $r=9$  cm, without rf bias. (b) Wave form of the voltage across the ground sheath,  $V_{gs}(t)$ , obtained at the same conditions.

For this reason, and for the sake of simplicity, the presheath will be considered part of the sheath in the remainder of this article.

Although ion collisions in the sheath can be neglected, ion collisions in the plasma cannot. In Fig. 2, the sampling cone is located at a radial position  $r=9$  cm. Ions created near  $r=0$ , the radial center of the discharge, undergo many collisions before reaching the sample cone sheath. Although Langmuir probe measurements<sup>29,30</sup> indicate that the plasma supports a radial electric field which accelerates  $\text{Ar}^+$  ions away from the center of the discharge, much of the momentum that ions gain from the field is redirected in random directions by  $\text{Ar}-\text{Ar}^+$  collisions. By assuming that the ions are in equilibrium with the local electric field, obtained from Miller's Langmuir probe data,<sup>29</sup> Hebner<sup>48</sup> calculated that  $\text{Ar}^+$  ions at radial positions of 4-8 cm have a radial drift velocity of about  $1 \times 10^5$  cm/s, which corresponds to an energy of only 0.2 eV. Laser-induced fluorescence measurements<sup>48</sup> of the drift velocity of argon metastable ions in the plasma were higher, ranging up to  $2.5 \times 10^5$  cm/s. This corresponds to an energy of 1.3 eV, which is still low compared to the energies in Fig. 2. Thus the ions gain nearly all of their energy in the sheath rather than the plasma.

Figure 2(b) shows the wave form of the voltage across the ground sheath,  $V_{gs}(t)$ , obtained at the same conditions as Fig. 2(a), using wire probe measurements and Eqs. (2)-(4). The voltage scale in Fig. 2(b) coincides with the energy scale of Fig. 2(a). The energy,  $E_0$ , of the peak in the energy distribution function closely corresponds to  $V_{dc}$ , the dc component of  $V_{gs}(t)$ . This observation confirms that the ions gain nearly all of their energy in the sheath rather than the plasma. Since no rf bias is applied, the only rf components observed in Fig. 2(b) are at the inductive source frequency and its harmonics. These components, which arise from a capacitive coupling between the inductive source and the plasma, are small, about 1 V, as noted in previous studies.<sup>27,29</sup> This 1 V modulation in  $V_{gs}(t)$  contributes to the width of the ion energy distribution. The distribution has a full-width at half-

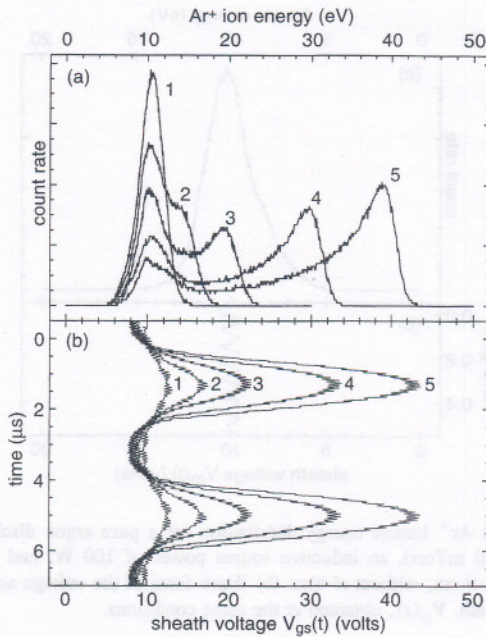


FIG. 3. (a) Ar<sup>+</sup> kinetic energy distribution for a pure argon discharge at 1.33 Pa (10 mTorr), an inductive source power of 100 W, a radial position  $r=9$  cm, and a bias frequency of 0.27 MHz, for varying rf bias amplitudes. (b) Wave forms of the voltage across the ground sheath,  $V_{gs}(t)$ , obtained under the same conditions.

maximum of 2.5 eV. About 1 eV of this width is contributed by the energy resolution of the energy analyzer. The remainder is contributed by the modulation in  $V_{gs}(t)$  and by the angular distribution of ion velocities within the plasma.

### B. Low frequency rf bias

Figure 3(a) shows ion energy distributions measured with rf bias applied at 0.27 MHz, at varying rf bias amplitudes. The distributions in Fig. 3(a) are broader than the distribution observed at zero rf bias [see Fig. 2(a)]. At the lowest rf bias amplitude, the distribution has a full-width at half-maximum of 3.3 eV, 0.8 eV broader than in Fig. 2(a). As the rf bias amplitude increases, the distribution continues to broaden and a double-peaked structure appears. The energy of the higher-energy peak increases with rf bias amplitude, but the position of the lower-energy peak remains constant. The lower-energy peak always lies close to  $E_0$ , the energy of the single peak in the distribution observed at zero rf bias [see Fig. 2(a)]. The double-peaked distributions are similar to previous measurements performed at low pressures and low frequencies.<sup>11,13,21,49</sup>

Figure 3(b) shows corresponding wave forms for the ground sheath voltage,  $V_{gs}(t)$ . The high frequency “ripple” visible in each wave form, independent of rf bias, is contributed by Fourier components at the inductive source frequency (13.56 MHz) and its harmonics, which are produced by capacitive coupling from the coil. The lower frequency features are contributed by Fourier components at the rf bias frequency and its harmonics. As the rf bias amplitude increases, the maximum wire probe voltage,  $V_{max}$ , becomes larger, reaching more than 40 V in Fig. 4(b), but the minimum wire probe voltage,  $V_{min}$ , decreases only slightly. This

behavior parallels that observed in Fig. 3(a). The energy of the higher-energy peak in the distributions,  $E_{high}$ , varies in the same manner as  $V_{max}$ ;  $E_{high}$  always lies a few electron volts below  $eV_{max}$  (where  $e$  is the charge of an electron). Similarly, the energy of the lower-energy peak in the distributions,  $E_{low}$ , lies a few electron volts above  $eV_{min}$ . The separation between the peaks,  $\Delta E_k$ , closely tracks the peak-to-peak amplitude of the ground sheath voltage,  $V_{pp}$ .

The correlations between Figs. 3(a) and 3(b) suggest that ions cross the sheath in front of the sampling cone rapidly compared to the time scale of Fig. 3(b). If so, ions entering the sheath at time  $t_0$ , when the instantaneous voltage across the sheath is  $V_{gs}(t_0)$ , will gain an energy  $eV_{gs}(t_0)$  in crossing the sheath. If they enter the sheath with low kinetic energies  $\ll eV_{gs}(t_0)$ , as argued in Sec. IV A above, they will exit the sheath and enter the mass spectrometer with a kinetic energy equal to  $eV_{gs}(t_0)$ . If ions enter the sheath at all times, then ions will be observed at all energies between  $eV_{max}$  and  $eV_{min}$ . The peaks at  $E_{max} \approx eV_{max}$  and  $E_{min} \approx eV_{min}$  are observed because  $V_{gs}(t)$  varies rather slowly near its maximum and minimum. Because  $V_{gs}(t)$  sweeps more rapidly through intermediate voltages, fewer ions are collected at intermediate energies.

The time it takes the ions to cross the sheath can be estimated using dc sheath models. The voltage drop across a dc sheath,  $V_0$ , is independent of time. At any position,  $x$ , in the sheath the potential,  $V(x)$ , is also independent of time. If the boundary between the plasma and the sheath is at  $x=0$  and if the electrode or other grounded surface is at  $x=W$ , then  $V(0)=V_0$ , and  $V(W)=0$ . If the ions have negligible initial velocity, then  $u(x)$ , the velocity of ions at position  $x$ , will be given by

$$\frac{1}{2} m_i u^2(x) = -eV(x) + eV_0, \quad (5)$$

where  $m_i$  is the ion mass. Using this equation, Poisson’s equation, and the ion continuity equation (with the electric field at  $x=0$ , the electron density in the sheath, and the density of other ionic species all set to zero) one can solve for  $V(x)$ . The solution is the Child–Langmuir law,<sup>50</sup>

$$x = \frac{2}{3} (2e/m_i)^{1/4} (\epsilon_0/J_0)^{1/2} [V_0 - V(x)]^{3/4}, \quad (6)$$

where  $\epsilon_0$  is the permittivity of vacuum and  $J_0$  is the ion current density. Evaluating Eq. (6) at  $x=W$ , one obtains

$$W = \frac{2}{3} (2e/m_i)^{1/4} (\epsilon_0/J_0)^{1/2} V_0^{3/4}. \quad (7)$$

Sometimes the ion transit time,  $\tau$ , is estimated by assuming ions cross the entire sheath at their maximum velocity,  $u_{max} = (2eV_0/m_i)^{1/2}$ . One obtains

$$\tau = W/u_{max} = \frac{2}{3} (m_i V_0/2e)^{1/4} (\epsilon_0/J_0)^{1/2}. \quad (8)$$

A more accurate estimate is obtained by integration. If  $y(t)$  is the position of an ion as a function of time, then the ion velocity as a function of time is  $dy/dt = u(y)$ , and the transit time is

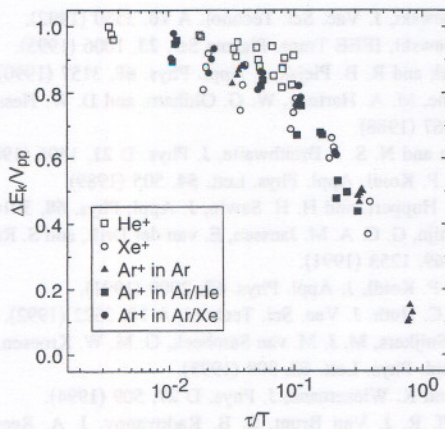


FIG. 12. Ratio of  $\Delta E_k$ , the separation between the high energy and low energy peaks in the ion energy distribution, to  $V_{pp}$ , the peak-to-peak ground sheath voltage, plotted vs  $\tau/T$ , where  $\tau$  is the ion transit time defined in Eq. (10) or Eq. (18) and  $T$  is the rf bias period. The data are from Figs. 5, 10 and 11. All data points obtained at  $V_{pp} > 20$  V are plotted.

We expect that the transit time of  $\text{Ar}^+$  would be unaffected by the presence of small quantities of helium or xenon. To calculate the transit time of  $\text{He}^+$  or  $\text{Xe}^+$ , the mass of He,  $m_{\text{He}}$ , or the mass of Xe,  $m_{\text{Xe}}$ , should be inserted into Eq. (9). Nevertheless, it is reasonable to assume that the voltage drop across the sheath should be determined by the dominant ion,  $\text{Ar}^+$ . Therefore, its mass,  $m_{\text{Ar}}$ , should be inserted into the Child–Langmuir law, Eq. (7). Solving, we obtain the transit time of  $\text{He}^+$ ,

$$\tau_{\text{He}} = 2(V_0/2em_{\text{Ar}})^{1/4}(m_{\text{He}}\epsilon_0/J_0)^{1/2}, \quad (18)$$

and the transit time of  $\text{Xe}^+$ ,  $\tau_{\text{Xe}}$ , given by a similar equation. According to this equation, the tenfold difference in mass between  $\text{He}^+$  and  $\text{Ar}^+$  results in values of  $\tau_{\text{He}}$  that are 0.32 times the transit time of  $\text{Ar}^+$ ,  $\tau_{\text{Ar}}$ . Similarly, the mass of  $\text{Xe}^+$  is 3.3 times greater than the mass of  $\text{Ar}^+$ , making  $\tau_{\text{Xe}}$  82% longer than  $\tau_{\text{Ar}}$ .

Data from both mixtures and pure argon are compared in Fig. 12. Transit times calculated from Eq. (10) for  $\text{Ar}^+$ , and Eq. (18) for  $\text{He}^+$  and  $\text{Xe}^+$ , are plotted on one axis. On the other axis is  $\Delta E_k/V_{pp}$ , the ratio of the separation between the high and low energy peaks,  $\Delta E_k$ , and the peak-to-peak amplitude of the ground sheath voltage,  $V_{pp}$ .  $\text{Ar}^+$  data from pure Ar, Ar/He, and Ar/Xe discharges fall close to a single curve. The  $\text{He}^+$  data and  $\text{Xe}^+$  data deviate more from the  $\text{Ar}^+$  curve. Part of the scatter in the data is due to systematic errors in the measurements. The error in the transit time values is estimated to be 25%, arising from a 50% uncertainty in the ion current density. We used an ion current density that was measured in a different inductively coupled GEC cell, under experimental conditions that were not identical to ours. Estimated errors in  $\Delta E_k$  and  $V_{pp}$  are each  $\pm 1$  V. The resulting error in  $\Delta E_k/V_{pp}$  is less than  $\pm 10\%$  for the data shown, which were all obtained at  $V_{pp} \geq 20$  V. (Data obtained at  $V_{pp} < 20$  V have larger relative errors in  $\Delta E_k/V_{pp}$ , but they are not plotted.) Errors may account for much of the spread in the data, but there are also real effects that could cause the data to deviate from a single curve. It is certainly possible that  $\Delta E_k$  is not solely a function of  $\tau/T$  and  $V_{pp}$ ; it

may also depend on other factors, such as the shape of the sheath voltage wave form. Thus, a single curve fitted to the data in Fig. 12 would not be expected to be perfectly general. Nevertheless such a curve could still provide useful estimates for  $\Delta E_k$  in situations where  $\Delta E_k$  is unknown but  $V_{pp}$  and  $\tau/T$  are known. For example, using the relation illustrated in Fig. 12 and measured values of the peak-to-peak voltage across the powered sheath, ion energies at the rf-biased electrode may be estimated.

## V. SUMMARY

Ion energy distributions at a grounded surface in an inductively coupled, high-density plasma reactor were measured and compared to measurements of the time-dependent sheath voltage that accelerates the ions. Together, the measurements provided a detailed characterization of the ion dynamics within the sheath. At 1.33 Pa (10 mTorr), ion energy distributions did not show any evidence of ion collisions within the sheath. Ion energy distributions were found to depend on three factors. The first factor was  $V_{bf}$ , the dc plasma potential in the absence of rf bias, which depends strongly on radial position and depends weakly on inductive source power. The energy of the single peak in the ion energy distribution observed when no rf bias was applied was approximately equal to  $eV_{bf}$ . The second factor was the amplitude of the ground sheath voltage, which depends strongly on the rf bias amplitude and rf bias frequency. The third factor was the ratio of the ion transit time to the rf period,  $\tau/T$ , which depends most strongly on the rf bias frequency and the ion mass. At low rf bias frequencies, where  $\tau/T < 0.05$ , the energies of the two peaks in the ion energy distribution observed when rf bias was applied,  $E_{\text{low}}$  and  $E_{\text{high}}$ , were approximately equal to the minimum and maximum ground sheath voltages. At higher rf bias frequencies, where  $\tau/T \approx 1$ ,  $E_{\text{high}}$  and  $E_{\text{low}}$  were approximately equal to the time-averaged sheath voltage. As the rf bias frequency increased, however, the discharge became more asymmetric, and the ground sheath voltage decreased. At high frequencies, the increasing asymmetry has a larger effect on ion energies than the changes in  $\tau/T$ . Sheath impedance models explain the increased asymmetry at high frequencies, and predict that it should occur at  $\tau/T \approx 0.1$ .

<sup>1</sup>J. H. Keller, J. C. Forster, and M. S. Barnes, *J. Vac. Sci. Technol. A* **11**, 2487 (1993).

<sup>2</sup>J. Asmussen, *J. Vac. Sci. Technol. A* **7**, 883 (1989).

<sup>3</sup>R. W. Boswell and R. K. Porteous, *Appl. Phys. Lett.* **50**, 1130 (1987).

<sup>4</sup>J. Hopwood, *Appl. Phys. Lett.* **62**, 940 (1993).

<sup>5</sup>U. Kortshagen and M. Zethoff, *Plasma Sources Sci. Technol.* **4**, 541 (1995).

<sup>6</sup>G. Mümken and U. Kortshagen, *J. Appl. Phys.* **80**, 6639 (1996).

<sup>7</sup>J. R. Woodworth, M. E. Riley, D. C. Meister, B. P. Aragon, M. S. Le, and H. H. Sawin, *J. Appl. Phys.* **80**, 1304 (1996).

<sup>8</sup>J. R. Woodworth, M. E. Riley, P. A. Miller, and T. W. Hamilton, *J. Appl. Phys.* **81**, 5950 (1997).

<sup>9</sup>J. R. Woodworth, M. E. Riley, P. A. Miller, C. A. Nichols, and T. W. Hamilton, *J. Vac. Sci. Technol. A* **15**, 3015 (1997).

<sup>10</sup>M. Matsuoka and K. Ono, *J. Vac. Sci. Technol. A* **6**, 25 (1987).

<sup>11</sup>W. M. Holber and J. Forster, *J. Vac. Sci. Technol. A* **8**, 3720 (1990).

<sup>12</sup>K. L. Junck and W. D. Getty, *J. Vac. Sci. Technol. A* **12**, 760 (1994).

<sup>13</sup>D. Martin and H. Oechsner, *Vacuum* **47**, 1017 (1996).

<sup>14</sup>G. W. Gibson, Jr., H. H. Sawin, I. Tepermeister, D. E. Ibbotson, and J. T. C. Lee, *J. Vac. Sci. Technol. B* **12**, 2333 (1994).  
<sup>15</sup>C. Charles, R. W. Boswell, and R. K. Porteous, *J. Vac. Sci. Technol. A* **398**, (1992).  
<sup>16</sup>C. Charles, *J. Vac. Sci. Technol. A* **11**, 157 (1993).  
<sup>17</sup>J. H. Kim and H. Y. Chang, *Phys. Plasmas* **3**, 1462 (1996).  
<sup>18</sup>Y. Ohtsu, G. Tochitani, H. Fujita, J. Zhang, Y. Setsuhara, and S. Miyake, *Jpn. J. Appl. Phys., Part 1* **36**, 4620 (1997).  
<sup>19</sup>Y. Okamoto and H. Tamagawa, *J. Phys. Soc. Jpn.* **29**, 187 (1970).  
<sup>20</sup>R. H. Bruce, *J. Appl. Phys.* **52**, 7064 (1981).  
<sup>21</sup>K. Kohler, D. E. Horne, and J. W. Coburn, *J. Appl. Phys.* **58**, 3350 (1985).  
<sup>22</sup>H. R. Koenig and L. I. Maissel, *IBM J. Res. Dev.* **14**, 168 (1970).  
<sup>23</sup>C. M. Horwitz, *J. Vac. Sci. Technol. A* **1**, 60 (1983).  
<sup>24</sup>K. Kohler, J. W. Coburn, D. E. Horne, E. Kay, and J. H. Keller, *J. Appl. Phys.* **57**, 59 (1985).  
<sup>25</sup>M. A. Lieberman, *J. Appl. Phys.* **65**, 4186 (1989).  
<sup>26</sup>M. A. Lieberman and S. E. Savas, *J. Vac. Sci. Technol. A* **8**, 1632 (1990).  
<sup>27</sup>M. A. Sobolewski, *Phys. Rev. E* **59**, 1059 (1999).  
<sup>28</sup>P. J. Hargis, Jr. *et al.*, *Rev. Sci. Instrum.* **65**, 140 (1994).  
<sup>29</sup>P. A. Miller, G. A. Hebner, K. E. Greenberg, P. D. Pochan, and B. P. Aragon, *J. Res. Natl. Inst. Stand. Technol.* **100**, 427 (1995).  
<sup>30</sup>A. Schwabedissen, E. C. Benck, and J. R. Roberts, *Phys. Rev. E* **55**, 3450 (1997).  
<sup>31</sup>The identification of commercial materials and their sources is made to foster understanding. In no case does this identification imply recommendation by the National Institute of Standards and Technology nor does it imply that the instrument is the best available.  
<sup>32</sup>J. K. Olthoff, R. J. Van Brunt, and S. B. Radovanov, *J. Appl. Phys.* **72**, 4566 (1992).  
<sup>33</sup>S. B. Radovanov, R. J. V. Brunt, J. K. Olthoff, and B. M. Jelenkovic, *Phys. Rev. E* **51**, 6036 (1995).

<sup>34</sup>M. A. Sobolewski, *J. Vac. Sci. Technol. A* **10**, 3550 (1992).  
<sup>35</sup>M. A. Sobolewski, *IEEE Trans. Plasma Sci.* **23**, 1006 (1995).  
<sup>36</sup>V. A. Godyak and R. B. Piejak, *J. Appl. Phys.* **68**, 3157 (1990).  
<sup>37</sup>W. M. Greene, M. A. Hartney, W. G. Oldham, and D. W. Hess, *J. Appl. Phys.* **63**, 1367 (1988).  
<sup>38</sup>S. G. Ingram and N. S. J. Braithwaite, *J. Phys. D* **21**, 1496 (1988).  
<sup>39</sup>C. Wild and P. Koidl, *Appl. Phys. Lett.* **54**, 505 (1989).  
<sup>40</sup>J. Liu, G. L. Huppert, and H. H. Sawin, *J. Appl. Phys.* **68**, 3916 (1990).  
<sup>41</sup>A. Manenschijn, G. C. A. M. Janssen, E. van der Drift, and S. Radelaar, *J. Appl. Phys.* **69**, 1253 (1991).  
<sup>42</sup>C. Wild and P. Koidl, *J. Appl. Phys.* **69**, 2909 (1991).  
<sup>43</sup>J. Janes and C. Huth, *J. Vac. Sci. Technol. A* **10**, 3522 (1992).  
<sup>44</sup>R. J. M. M. Snijders, M. J. M. van Sambeek, G. M. W. Kroesen, and F. J. de Hoog, *Appl. Phys. Lett.* **63**, 308 (1993).  
<sup>45</sup>U. Flender and K. Wiesemann, *J. Phys. D* **27**, 509 (1994).  
<sup>46</sup>J. K. Olthoff, R. J. Van Brunt, S. B. Radovanov, J. A. Rees, and R. Surowiec, *J. Appl. Phys.* **75**, 115 (1994).  
<sup>47</sup>M. V. V. S. Rao, R. J. Van Brunt, and J. K. Olthoff, *Phys. Rev. E* **54**, 5641 (1996).  
<sup>48</sup>G. A. Hebner, *J. Appl. Phys.* **80**, 2624 (1996).  
<sup>49</sup>J. W. Coburn and E. Kay, *J. Appl. Phys.* **43**, 4965 (1972).  
<sup>50</sup>C. D. Child, *Phys. Rev.* **32**, 492 (1911).  
<sup>51</sup>M. J. Kushner, *J. Appl. Phys.* **58**, 4024 (1985).  
<sup>52</sup>M. S. Barnes, J. C. Forster, and J. H. Keller, *IEEE Trans. Plasma Sci.* **19**, 240 (1991).  
<sup>53</sup>M. A. Lieberman, *IEEE Trans. Plasma Sci.* **16**, 638 (1988).  
<sup>54</sup>R. J. Hoekstra and M. J. Kushner, *J. Appl. Phys.* **79**, 2275 (1996).  
<sup>55</sup>J. K. Olthoff, R. J. Van Brunt, S. B. Radovanov, and J. A. Rees, *IEE Proc. Sci. Meas. Technol.* **141**, 105 (1994).

approximately equal to  $V_{0.5}$ . The second factor was the ratio of the ground sheath voltage, which depends strongly on the  $r$  bias amplitude and  $r$  bias frequency. The third factor was the ratio of the ion transit time to the  $r$  bias frequency, which depends most strongly on the  $r$  bias frequency and the ion mass. At low  $r$  bias frequencies, where  $\omega r \ll v_{Te}$ , the energies of the two peaks in the ion energy distribution observed when  $r$  bias was applied,  $E_{low}$  and  $E_{high}$ , were approximately equal to the minimum and maximum ground sheath voltage. At higher  $r$  bias frequencies, where  $\omega r \gg v_{Te}$ ,  $E_{low}$  and  $E_{high}$  were approximately equal to the time-averaged sheath voltage. As the  $r$  bias frequency increased, however, the discharge became more asymmetric and the ground sheath voltage decreased. At high frequencies, the increasing asymmetry has a larger effect on ion energies than the changes in  $V_T$ . Sheath impedance models explain the increased asymmetry at high frequencies, and predict that it should occur at  $\omega r \sim 0.1$ .

and the transit time of  $Xe^+$ ,  $\tau_{tr}$ , given by a similar equation. According to this equation, the ion-to-ion difference in mass between  $He^+$  and  $Ar^+$  results in values of  $\tau_{tr}$  that are 0.33 times the transit time of  $Ar^+$ . Similarly, the mass of  $Xe^+$  is 3.3 times greater than the mass of  $Ar^+$ , making  $\tau_{tr}$  3.3% larger than  $\tau_{tr}^{Ar}$ . Data from both ionizers and pure argon are compared in Fig. 17. Transit times calculated from Eq. (10) for  $Ar^+$  and  $He^+$  (18) for  $He^+$  and  $Xe^+$  are plotted on one axis. On the other axis is  $\Delta E_{low}/V_{0.5}$ , the ratio of the separation between the high and low energy peaks,  $\Delta E_{low}$ , and the peak-to-peak amplitude of the ground sheath voltage,  $V_{0.5}$ .  $Ar^+$  data from pure  $Ar$  and  $Ar/Xe$  discharges fall close to a single curve. The  $He^+$  data and  $Xe^+$  data deviate more from the  $Ar^+$  curve than do the data in the data in the case of systematic errors in the measurements. The error in the transit time due to the error in the ion current density,  $W$ , used as ion current density that was measured in a different ionizer, is not expected to be a major experimental condition that was not included in our. Estimated errors in  $\Delta E_{low}$  and  $V_{0.5}$  are each  $\pm 1$  V. The resulting error in  $\Delta E_{low}/V_{0.5}$  is less than  $\pm 10\%$  for the data shown, which were all obtained at  $V_{0.5} > 30$  V. Data obtained at  $V_{0.5} < 30$  V have larger relative errors in  $\Delta E_{low}/V_{0.5}$ , but they are not plotted; errors may account for much of the spread in the data, but there are also real effects that could cause the data to deviate from a single curve. It is certainly possible that  $\Delta E_{low}$  is not only a function of  $\omega r$  and  $V_{0.5}$ , it





$$\frac{V_{gs}}{V_{ps}} = \frac{1 - \cos(\omega t_{gs}/2)}{1 - \cos(\omega t_{ps}/2)} \approx \left(\frac{t_{gs}}{t_{ps}}\right)^2 = \left(\frac{J_{ps} A_{ps}}{J_{gs} A_{gs}}\right)^2. \quad (15)$$

The power law exponent of  $A_{ps}/A_{gs}$  in Eq. (15) is lower than in Eq. (13), indicating that discharges are more symmetric for low-frequency, resistive sheaths than for high-frequency, capacitive sheaths. In Eq. (15) the dependence on area ratio has the same power law as the dependence on ion current density. The ion current density at the powered electrode is greater than the ion current density at grounded surfaces, which are farther from the center of the discharge. Therefore, the ion current factors tend to make  $V_{gs}/V_{ps}$  larger, counteracting the area factors, which tend to make  $V_{gs}/V_{ps}$  smaller. Indeed, in some cases at 0.27 MHz the peak-to-peak amplitude of  $V_{gs}(t)$  was larger than the peak-to-peak amplitude of  $V_{ps}(t)$ . This was only observed when the steel plate was placed on the lower electrode, which greatly increases its area,  $A_{ps}$ . With the steel plate removed, smaller values of  $V_{gs}/V_{ps}$  were observed. The data in Figs. 2–7 were obtained with the steel plate; data in the remaining figures were obtained without it.

The transition between the low frequency regime of Eq. (15) and the high-frequency regime of Eq. (13) occurs at a frequency  $\omega_c$ , which can be defined as the frequency at which the magnitude of the displacement current flowing through the ground sheath,  $V_{gs1}/Z_{gs}$ , equals the conduction current flowing through the ground sheath,  $J_{gs}A_{gs}$ . Using Eqs. (10) and (12), one obtains

$$\omega_c \tau = 3/4. \quad (16)$$

Alternatively, the transition can be considered to occur at an rf period,  $T_c = 2\pi/\omega_c$ , where

$$\tau/T_c = 3/8\pi = 0.12. \quad (17)$$

Thus the transition to capacitive sheath impedances and the resulting increase in the asymmetry of the discharge occurs at values of  $\tau/T$  which are quite close to the range where ion transit time effects begin to narrow the ion energy distribution. Thus, it is no accident that the narrowing of the ion energy distribution due to ion transit time effects and the increase in discharge asymmetry are observed in the same frequency range.

### E. Dependence on inductive source power

In Fig. 8, the energies of the peaks in the ion energy distribution,  $E_{high}$  and  $E_{low}$ , are plotted as a function of the peak-to-peak ground sheath voltage, at two different rf bias frequencies and two different inductive source powers. At either frequency, an increase in inductive source power from 75 to 250 W produces an increase in  $E_{high}$  and  $E_{low}$ . The increase is approximately 2 V, for  $E_{high}$  as well as  $E_{low}$ , at 0.27 MHz as well as 1.00 MHz, and for all values of the ground sheath voltage. These results are consistent with Miller's Langmuir probe measurements of the dc plasma potential in argon discharges in his inductive GEC cell.<sup>29</sup> Miller's data show that the dc plasma potential at a radial position  $r=9$  cm (corresponding to the position of the sampling cone) increases by 2 V, from 9 to 11 V, as the source power rises from 77 to 245 W. (It should be noted that Miller re-

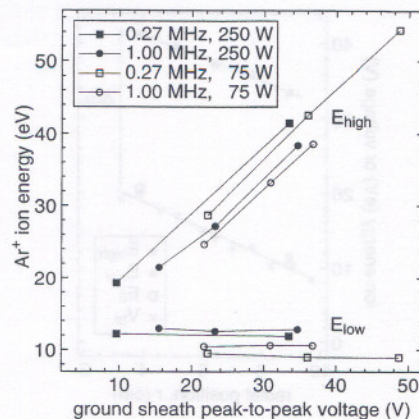


FIG. 8. Energy of the higher energy peak in the  $Ar^+$  distribution,  $E_{high}$ , and the lower energy peak,  $E_{low}$ , as a function of  $V_{pp}$ , the peak-to-peak amplitude of the ground sheath voltage, for rf bias frequencies of 0.27 and 1.00 MHz, and inductive source powers of 75 and 250 W. Data were obtained for a pure argon discharge at 1.33 Pa (10 mTorr), at a radial position  $r=9$  cm, with no steel plate on the lower electrode.

ports source powers after subtracting an estimate of the power lost due to the resistance of the inductive source, whereas we report the total power at the generator, which includes resistive losses.) As the source power increases, the increase in dc plasma potential is accompanied by a simultaneous increase in the electron temperature.<sup>29</sup> The dc plasma potential must increase if the electron temperature increases, because the current carried by electrons leaving the plasma must remain equal to the current carried by ions leaving the plasma.

Ion currents measured in argon discharges in the inductively coupled GEC cell are roughly proportional to the inductive source power.<sup>27</sup> If the ion current increases the sheath width and transit times will decrease, according to Eqs. (7) and (10). For the increase in source power given in Fig. 8, the transit time should decrease by a factor of about 1.8. A change in the ion transit time will not affect the ion energies if the rf period is much greater than or much less than the ion transit time, but it will affect the ion energies if the rf period and the transit time are comparable. This possible dependence of ion energy on inductive source power has been discussed previously.<sup>54</sup> Nevertheless, we see no evidence of this effect in Fig. 8. No significant changes in the slope of the plots in Fig. 8 are observed, perhaps because the rf bias frequencies are too low, the rf period too long, and the transit time too short. It was difficult to investigate higher frequencies, because of the increase in discharge asymmetry discussed above in Sec. IV D and Fig. 7.

### F. Dependence on position

Figure 9 shows ion energy parameters measured as a function of the radial position of the sampling orifice. The measurements were performed at constant inductive source power (130 W) and constant rf bias frequency (2.0 MHz). The rf bias amplitude was adjusted to maintain a constant peak-to-peak ground sheath voltage,  $V_{pp}=30$  V, except for two measurements which were performed with the rf bias turned off. The radial position,  $r$ , of the entrance orifice of

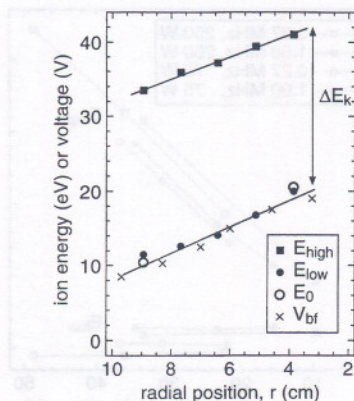


FIG. 9. Energy of the higher energy peak in the  $\text{Ar}^+$  distribution,  $E_{\text{high}}$ , and the lower energy peak,  $E_{\text{low}}$ , as a function of  $r$ , the radial position of the mass spectrometer sampling cone, for a discharge in pure argon at 1.33 Pa (10 mTorr), an inductive source power of 130 W, and an rf bias frequency of 2 MHz. Also plotted are the energy of the single peak,  $E_0$ , observed when no rf bias was applied, and values from Ref. 29 of the dc plasma potential,  $V_{\text{bf}}$ , measured by a Langmuir probe.

the mass spectrometer relative to the radial center of the discharge cell was varied from 4 to 9 cm. Also shown are measurements<sup>29</sup> of the dc plasma potential at zero rf bias,  $V_{\text{bf}}$ , obtained by moving a Langmuir probe through the same region. The slope of  $V_{\text{bf}}$  indicates that the plasma sustains a radial electric field of 1.7 V/cm. But the energy that ions gain from this field is mostly lost due to  $\text{Ar}-\text{Ar}^+$  collisions in the plasma, as discussed in Sec. IV A, above. Consequently, the energy of the single peak observed at zero rf bias,  $E_0$ , plotted in Fig. 9, corresponds closely to the dc plasma potential,  $V_{\text{bf}}$ . Similarly,  $E_{\text{low}}$ , the energy of the lower energy peak observed when rf bias is applied, also tracks  $V_{\text{bf}}$ .

The plot of  $E_{\text{high}}$ , the energy of the higher energy peak observed when rf bias is applied, lies parallel to the plot of  $E_{\text{low}}$ , so that their difference,  $\Delta E_k = E_{\text{high}} - E_{\text{low}}$ , remains constant. This observation confirms that the components of the plasma potential at the rf bias frequency and its harmonics do not vary radially. If they did, they would produce variations in the peak-to-peak ground sheath voltage and in  $\Delta E_k$ .

Measurements in the inductively coupled GEC cell show that the ion current density increases as one moves towards  $r=0$ , the center of the discharge.<sup>7</sup> Thus one would expect the transit time through the sampling cone sheath to be smaller when the cone was positioned closer to  $r=0$ . If the transit time were comparable to the rf period, this decrease in transit time would produce an increase in  $\Delta E_k$  as one moved towards  $r=0$ . This effect is not observed, because, presumably, the rf bias frequency is too low, so that the transit time is much smaller than the rf period. It was difficult to investigate higher frequencies because of the increase in discharge asymmetry discussed above in Sec. IV D.

### G. Dependence on ion mass

In studies of low-density, capacitively coupled discharges<sup>19,49</sup> it has been observed that ion energy distributions of heavier ions are narrower than lighter ions. Heavy

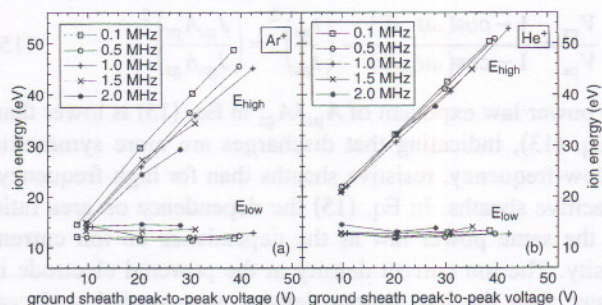


FIG. 10. Energy of the high and low energy peaks,  $E_{\text{high}}$  and  $E_{\text{low}}$ , in the (a)  $\text{Ar}^+$  and (b)  $\text{He}^+$  ion energy distribution, as a function of  $V_{\text{pp}}$ , the peak-to-peak amplitude of the ground sheath voltage, for varying rf bias frequencies. Data were obtained for an argon/helium discharge at 1.33 Pa (10 mTorr), at an argon flow of 2.5 sccm, a helium flow of 2.5 sccm, an inductive source power of 130 W, and a radial position  $r=9$  cm, with no steel plate on the lower electrode.

ions are not accelerated as rapidly as light ions, so they have longer transit times, and hence narrower energy distributions.

To study ion mass effects, experiments were performed with mixtures. Figure 10 shows data obtained from mixtures of argon and helium. The flow rates of argon and helium were equal (2.5 sccm). Nevertheless,  $\text{Ar}^+$  ions far outnumbered  $\text{He}^+$ , as one would expect, since helium has a higher ionization potential than argon. (Furthermore, when He is added, the production of  $\text{Ar}^+$  actually increases, due to Penning ionization.)<sup>55</sup> The  $\text{Ar}^+$  data, shown in Fig. 10(a), are very similar to results from pure argon (Fig. 5). In comparison, for  $\text{He}^+$ , shown in Fig. 10(b),  $E_{\text{high}}$  is higher,  $E_{\text{low}}$  is lower, and the spread  $\Delta E_k = E_{\text{high}} - E_{\text{low}}$  is wider. There does not seem to be any frequency dependence in the  $\text{He}^+$  data, which suggests that the transit time of  $\text{He}^+$ ,  $\tau_{\text{He}}$ , is much smaller than the rf period,  $T$ . Measurements performed in mixtures of argon (50 sccm) with small quantities of xenon (1 sccm) are shown in Fig. 11. The energies of the peaks of the  $\text{Ar}^+$  energy distribution, shown in Fig. 11(a), do not differ from pure argon (Fig. 4) or argon-helium mixtures [Fig. 10(a)]. In comparison, for  $\text{Xe}^+$ , shown in Fig. 11(b),  $E_{\text{high}}$  is lower,  $E_{\text{low}}$  is higher, and the spread  $\Delta E_k = E_{\text{high}} - E_{\text{low}}$  is narrower, suggesting that  $\text{Xe}^+$ , because of its higher mass, has a longer transit time.

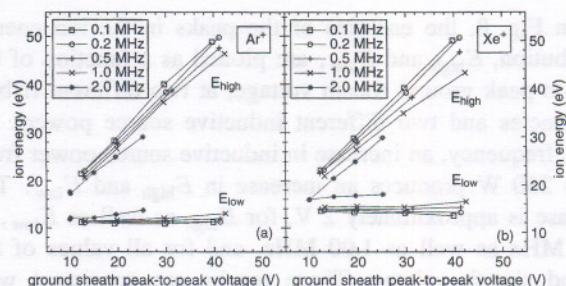


FIG. 11. Energy of the high and low energy peaks,  $E_{\text{high}}$  and  $E_{\text{low}}$ , in the (a)  $\text{Ar}^+$  and (b)  $\text{Xe}^+$  ion energy distribution, as a function of  $V_{\text{pp}}$ , the peak-to-peak amplitude of the ground sheath voltage, for varying rf bias frequencies. Data were obtained for an argon/xenon discharge at 1.33 Pa (10 mTorr), at an argon flow of 50.0 sccm, a xenon flow of 1.0 sccm, an inductive source power of 130 W, and a radial position  $r=9$  cm, with no steel plate on the lower electrode.

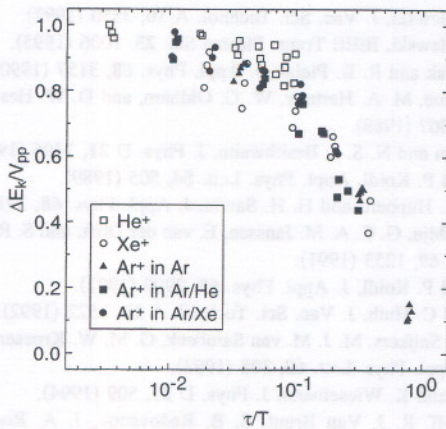


FIG. 12. Ratio of  $\Delta E_k$ , the separation between the high energy and low energy peaks in the ion energy distribution, to  $V_{pp}$ , the peak-to-peak ground sheath voltage, plotted vs  $\tau/T$ , where  $\tau$  is the ion transit time defined in Eq. (10) or Eq. (18) and  $T$  is the rf bias period. The data are from Figs. 5, 10 and 11. All data points obtained at  $V_{pp} > 20$  V are plotted.

We expect that the transit time of  $\text{Ar}^+$  would be unaffected by the presence of small quantities of helium or xenon. To calculate the transit time of  $\text{He}^+$  or  $\text{Xe}^+$ , the mass of He,  $m_{\text{He}}$ , or the mass of Xe,  $m_{\text{Xe}}$ , should be inserted into Eq. (9). Nevertheless, it is reasonable to assume that the voltage drop across the sheath should be determined by the dominant ion,  $\text{Ar}^+$ . Therefore, its mass,  $m_{\text{Ar}}$ , should be inserted into the Child-Langmuir law, Eq. (7). Solving, we obtain the transit time of  $\text{He}^+$ ,

$$\tau_{\text{He}} = 2(V_0/2em_{\text{Ar}})^{1/4}(m_{\text{He}}\epsilon_0/J_0)^{1/2}, \quad (18)$$

and the transit time of  $\text{Xe}^+$ ,  $\tau_{\text{Xe}}$ , given by a similar equation. According to this equation, the tenfold difference in mass between  $\text{He}^+$  and  $\text{Ar}^+$  results in values of  $\tau_{\text{He}}$  that are 0.32 times the transit time of  $\text{Ar}^+$ ,  $\tau_{\text{Ar}}$ . Similarly, the mass of  $\text{Xe}^+$  is 3.3 times greater than the mass of  $\text{Ar}^+$ , making  $\tau_{\text{Xe}}$  82% longer than  $\tau_{\text{Ar}}$ .

Data from both mixtures and pure argon are compared in Fig. 12. Transit times calculated from Eq. (10) for  $\text{Ar}^+$ , and Eq. (18) for  $\text{He}^+$  and  $\text{Xe}^+$ , are plotted on one axis. On the other axis is  $\Delta E_k/V_{pp}$ , the ratio of the separation between the high and low energy peaks,  $\Delta E_k$ , and the peak-to-peak amplitude of the ground sheath voltage,  $V_{pp}$ .  $\text{Ar}^+$  data from pure Ar, Ar/He, and Ar/Xe discharges fall close to a single curve. The  $\text{He}^+$  data and  $\text{Xe}^+$  data deviate more from the  $\text{Ar}^+$  curve. Part of the scatter in the data is due to systematic errors in the measurements. The error in the transit time values is estimated to be 25%, arising from a 50% uncertainty in the ion current density. We used an ion current density that was measured in a different inductively coupled GEC cell, under experimental conditions that were not identical to ours. Estimated errors in  $\Delta E_k$  and  $V_{pp}$  are each  $\pm 1$  V. The resulting error in  $\Delta E_k/V_{pp}$  is less than  $\pm 10\%$  for the data shown, which were all obtained at  $V_{pp} \geq 20$  V. (Data obtained at  $V_{pp} < 20$  V have larger relative errors in  $\Delta E_k/V_{pp}$ , but they are not plotted.) Errors may account for much of the spread in the data, but there are also real effects that could cause the data to deviate from a single curve. It is certainly possible that  $\Delta E_k$  is not solely a function of  $\tau/T$  and  $V_{pp}$ ; it

may also depend on other factors, such as the shape of the sheath voltage wave form. Thus, a single curve fitted to the data in Fig. 12 would not be expected to be perfectly general. Nevertheless such a curve could still provide useful estimates for  $\Delta E_k$  in situations where  $\Delta E_k$  is unknown but  $V_{pp}$  and  $\tau/T$  are known. For example, using the relation illustrated in Fig. 12 and measured values of the peak-to-peak voltage across the powered sheath, ion energies at the rf-biased electrode may be estimated.

## V. SUMMARY

Ion energy distributions at a grounded surface in an inductively coupled, high-density plasma reactor were measured and compared to measurements of the time-dependent sheath voltage that accelerates the ions. Together, the measurements provided a detailed characterization of the ion dynamics within the sheath. At 1.33 Pa (10 mTorr), ion energy distributions did not show any evidence of ion collisions within the sheath. Ion energy distributions were found to depend on three factors. The first factor was  $V_{bf}$ , the dc plasma potential in the absence of rf bias, which depends strongly on radial position and depends weakly on inductive source power. The energy of the single peak in the ion energy distribution observed when no rf bias was applied was approximately equal to  $eV_{bf}$ . The second factor was the amplitude of the ground sheath voltage, which depends strongly on the rf bias amplitude and rf bias frequency. The third factor was the ratio of the ion transit time to the rf period,  $\tau/T$ , which depends most strongly on the rf bias frequency and the ion mass. At low rf bias frequencies, where  $\tau/T < 0.05$ , the energies of the two peaks in the ion energy distribution observed when rf bias was applied,  $E_{\text{low}}$  and  $E_{\text{high}}$ , were approximately equal to the minimum and maximum ground sheath voltages. At higher rf bias frequencies, where  $\tau/T \approx 1$ ,  $E_{\text{high}}$  and  $E_{\text{low}}$  were approximately equal to the time-averaged sheath voltage. As the rf bias frequency increased, however, the discharge became more asymmetric, and the ground sheath voltage decreased. At high frequencies, the increasing asymmetry has a larger effect on ion energies than the changes in  $\tau/T$ . Sheath impedance models explain the increased asymmetry at high frequencies, and predict that it should occur at  $\tau/T \approx 0.1$ .

<sup>1</sup>J. H. Keller, J. C. Forster, and M. S. Barnes, *J. Vac. Sci. Technol. A* **11**, 2487 (1993).

<sup>2</sup>J. Asmussen, *J. Vac. Sci. Technol. A* **7**, 883 (1989).

<sup>3</sup>R. W. Boswell and R. K. Porteous, *Appl. Phys. Lett.* **50**, 1130 (1987).

<sup>4</sup>J. Hopwood, *Appl. Phys. Lett.* **62**, 940 (1993).

<sup>5</sup>U. Kortshagen and M. Zethoff, *Plasma Sources Sci. Technol.* **4**, 541 (1995).

<sup>6</sup>G. Mümken and U. Kortshagen, *J. Appl. Phys.* **80**, 6639 (1996).

<sup>7</sup>J. R. Woodworth, M. E. Riley, D. C. Meister, B. P. Aragon, M. S. Le, and H. H. Sawin, *J. Appl. Phys.* **80**, 1304 (1996).

<sup>8</sup>J. R. Woodworth, M. E. Riley, P. A. Miller, and T. W. Hamilton, *J. Appl. Phys.* **81**, 5950 (1997).

<sup>9</sup>J. R. Woodworth, M. E. Riley, P. A. Miller, C. A. Nichols, and T. W. Hamilton, *J. Vac. Sci. Technol. A* **15**, 3015 (1997).

<sup>10</sup>M. Matsuoka and K. Ono, *J. Vac. Sci. Technol. A* **6**, 25 (1987).

<sup>11</sup>W. M. Holber and J. Forster, *J. Vac. Sci. Technol. A* **8**, 3720 (1990).

<sup>12</sup>K. L. Junck and W. D. Getty, *J. Vac. Sci. Technol. A* **12**, 760 (1994).

<sup>13</sup>D. Martin and H. Oechsner, *Vacuum* **47**, 1017 (1996).

<sup>14</sup>G. W. Gibson, Jr., H. H. Sawin, I. Tepermeister, D. E. Ibbotson, and J. T. C. Lee, *J. Vac. Sci. Technol. B* **12**, 2333 (1994).

<sup>15</sup>C. Charles, R. W. Boswell, and R. K. Porteous, *J. Vac. Sci. Technol. A* **398**, (1992).

<sup>16</sup>C. Charles, *J. Vac. Sci. Technol. A* **11**, 157 (1993).

<sup>17</sup>J. H. Kim and H. Y. Chang, *Phys. Plasmas* **3**, 1462 (1996).

<sup>18</sup>Y. Ohtsu, G. Tochitani, H. Fujita, J. Zhang, Y. Setsuhara, and S. Miyake, *Jpn. J. Appl. Phys., Part 1* **36**, 4620 (1997).

<sup>19</sup>Y. Okamoto and H. Tamagawa, *J. Phys. Soc. Jpn.* **29**, 187 (1970).

<sup>20</sup>R. H. Bruce, *J. Appl. Phys.* **52**, 7064 (1981).

<sup>21</sup>K. Kohler, D. E. Horne, and J. W. Coburn, *J. Appl. Phys.* **58**, 3350 (1985).

<sup>22</sup>H. R. Koenig and L. I. Maissel, *IBM J. Res. Dev.* **14**, 168 (1970).

<sup>23</sup>C. M. Horwitz, *J. Vac. Sci. Technol. A* **1**, 60 (1983).

<sup>24</sup>K. Kohler, J. W. Coburn, D. E. Horne, E. Kay, and J. H. Keller, *J. Appl. Phys.* **57**, 59 (1985).

<sup>25</sup>M. A. Lieberman, *J. Appl. Phys.* **65**, 4186 (1989).

<sup>26</sup>M. A. Lieberman and S. E. Savas, *J. Vac. Sci. Technol. A* **8**, 1632 (1990).

<sup>27</sup>M. A. Sobolewski, *Phys. Rev. E* **59**, 1059 (1999).

<sup>28</sup>P. J. Hargis, Jr. *et al.*, *Rev. Sci. Instrum.* **65**, 140 (1994).

<sup>29</sup>P. A. Miller, G. A. Hebner, K. E. Greenberg, P. D. Pochan, and B. P. Aragon, *J. Res. Natl. Inst. Stand. Technol.* **100**, 427 (1995).

<sup>30</sup>A. Schwabedissen, E. C. Benck, and J. R. Roberts, *Phys. Rev. E* **55**, 3450 (1997).

<sup>31</sup>The identification of commercial materials and their sources is made to foster understanding. In no case does this identification imply recommendation by the National Institute of Standards and Technology nor does it imply that the instrument is the best available.

<sup>32</sup>J. K. Olthoff, R. J. Van Brunt, and S. B. Radovanov, *J. Appl. Phys.* **72**, 4566 (1992).

<sup>33</sup>S. B. Radovanov, R. J. V. Brunt, J. K. Olthoff, and B. M. Jelenkovic, *Phys. Rev. E* **51**, 6036 (1995).

<sup>34</sup>M. A. Sobolewski, *J. Vac. Sci. Technol. A* **10**, 3550 (1992).

<sup>35</sup>M. A. Sobolewski, *IEEE Trans. Plasma Sci.* **23**, 1006 (1995).

<sup>36</sup>V. A. Godyak and R. B. Piejak, *J. Appl. Phys.* **68**, 3157 (1990).

<sup>37</sup>W. M. Greene, M. A. Hartney, W. G. Oldham, and D. W. Hess, *J. Appl. Phys.* **63**, 1367 (1988).

<sup>38</sup>S. G. Ingram and N. S. J. Braithwaite, *J. Phys. D* **21**, 1496 (1988).

<sup>39</sup>C. Wild and P. Koidl, *Appl. Phys. Lett.* **54**, 505 (1989).

<sup>40</sup>J. Liu, G. L. Huppert, and H. H. Sawin, *J. Appl. Phys.* **68**, 3916 (1990).

<sup>41</sup>A. Manenschijn, G. C. A. M. Janssen, E. van der Drift, and S. Radelaar, *J. Appl. Phys.* **69**, 1253 (1991).

<sup>42</sup>C. Wild and P. Koidl, *J. Appl. Phys.* **69**, 2909 (1991).

<sup>43</sup>J. Janes and C. Huth, *J. Vac. Sci. Technol. A* **10**, 3522 (1992).

<sup>44</sup>R. J. M. M. Sniijkers, M. J. M. van Sambeek, G. M. W. Kroesen, and F. J. de Hoog, *Appl. Phys. Lett.* **63**, 308 (1993).

<sup>45</sup>U. Flender and K. Wiesemann, *J. Phys. D* **27**, 509 (1994).

<sup>46</sup>J. K. Olthoff, R. J. Van Brunt, S. B. Radovanov, J. A. Rees, and R. Surowiec, *J. Appl. Phys.* **75**, 115 (1994).

<sup>47</sup>M. V. V. S. Rao, R. J. Van Brunt, and J. K. Olthoff, *Phys. Rev. E* **54**, 5641 (1996).

<sup>48</sup>G. A. Hebner, *J. Appl. Phys.* **80**, 2624 (1996).

<sup>49</sup>J. W. Coburn and E. Kay, *J. Appl. Phys.* **43**, 4965 (1972).

<sup>50</sup>C. D. Child, *Phys. Rev.* **32**, 492 (1911).

<sup>51</sup>M. J. Kushner, *J. Appl. Phys.* **58**, 4024 (1985).

<sup>52</sup>M. S. Barnes, J. C. Forster, and J. H. Keller, *IEEE Trans. Plasma Sci.* **19**, 240 (1991).

<sup>53</sup>M. A. Lieberman, *IEEE Trans. Plasma Sci.* **16**, 638 (1988).

<sup>54</sup>R. J. Hoekstra and M. J. Kushner, *J. Appl. Phys.* **79**, 2275 (1996).

<sup>55</sup>J. K. Olthoff, R. J. Van Brunt, S. B. Radovanov, and J. A. Rees, *IEE Proc. Sci. Meas. Technol.* **141**, 105 (1994).



